Research Square

Preprints are preliminary reports that have not undergone peer review.
They should not be considered conclusive, used to inform clinical practice,
or referenced by the media as validated information.

Influence of Bottom Electrode Material on the Morphological and Frequency-Dependent Electrical Characteristics of Sputtered HfO_2 Thin-Film Metal-Insulator-Metal Capacitors

Abdullah

p22ee001@iitj.ac.in

Indian Institute of Technology Jodhpur https://orcid.org/0000-0001-9487-2595

Research Article

Keywords: HfO_2 thin films, Metal–insulator–metal capacitors, RF magnetron sputtering, Bottom electrode, Dielectric constant, Frequency-dependent electrical characteristics

Posted Date: July 10th, 2026

DOI: https://doi.org/10.21203/rs.3.rs-10296707/v1

License: This work is licensed under a Creative Commons Attribution 4.0 International License.
Read Full License

Additional Declarations: The authors declare no competing interests.

Influence of Bottom Electrode Material on the Morphological and Frequency-Dependent Electrical Characteristics of Sputtered HfO_2 Thin-Film Metal-Insulator-Metal Capacitors

Abdullah[1*]
[1]*Department of Electronics Engineering*
[1]*Indian Institute of Technology Jodhpur, Jodhpur-342030, Rajasthan, India*
**Corresponding Author p22ee001@iitj.ac.in*

Abstract

The influence of bottom electrode material on the morphological and frequency-dependent electrical characteristics of RF-sputtered HfO_2 thin-film metal–insulator–metal (MIM) capacitors was systematically investigated. Two capacitor structures, namely Al/HfO_2/Pt and Al/HfO_2/Al, were fabricated by depositing a 100 nm HfO_2 dielectric layer using RF magnetron sputtering on platinized Si and Al-coated SiO_2 substrates, respectively. Further, circular aluminum top electrodes with a thickness of 300 nm and a diameter of 500 μm were deposited by thermal evaporation technique using shadow mask. The surface morphologies were characterized by atomic force microscope (AFM). The electrical properties were measured by Keithley 4200A-SCS semiconductor parameter analyzer by C-V and G-V measurements for voltage sweep ranges ±2 V, ±5 V, and ±10 V with frequencies of 100 kHz to 1 MHz. By AFM measurements, it has been found that HfO_2 thin films had smooth and uniform morphologies with RMS roughness of 4.40 nm and 4.90 nm for Pt- and Al-based structures, respectively. It is found that both capacitors had normal frequency dependence with capacitance, dielectric constant, capacitance density, dielectric loss, quality factor, conductance, and parallel resistance depend strongly on the measurement frequency. On the contrary, the Al/HfO_2/Pt structure showed relatively low dielectric loss, higher quality factor, high parallel resistance, and better surface morphology, indicating good dielectric insulator property and low dissipation of energy. The conclusion drawn from these studies is that bottom electrode material determines the properties of dielectric/electrode interface and controls the frequency dependent electrical characteristics of sputtered HfO_2 thin film MIM capacitors. This knowledge will be helpful in designing HfO_2 based dielectric capacitors for high frequency analog and RF applications.

Keywords: HfO_2 thin films; Metal–insulator–metal capacitors; RF magnetron sputtering; Bottom electrode; Dielectric constant; Frequency-dependent electrical characteristics.

1. Introduction

The advancement in microelectronics and communication technologies as well as the development of IC fabrication technologies has substantially boosted the demands for smaller electronic devices that operate at faster speeds and consume lesser energy besides being more reliable and having higher integration densities. The shrinking trend of semiconductor devices under Moore's law has led to the need for stringent specifications on the dielectric materials employed in capacitors, transistors, RF circuits, and memories. The commonly used conventional silicon dioxide (SiO_2) as a dielectric material has been rendered impractical due to its scaling limit since its aggressive reduction leads to significant tunneling leakage currents, reduced dielectric reliability, and power losses. Hence, extensive research work has been carried out with the aim of replacing the conventional SiO_2 with other high dielectric constant (high-k) materials to offer higher capacitance values with physically thick insulator layers. Such high-k dielectrics are essential for minimizing leakage current, achieving better electrostatic control, and improving device reliability without violating scaling demands **[1-5]**.

Of all the possible high-k dielectrics studied during the last two decades, one of the most interesting is hafnium oxide (HfO_2), which is characterized by an exceptional combination of electrical, physical, and chemical properties. HfO_2 features relatively high dielectric constant (around 20–25), relatively wide band gap (around 5.7–5.9 eV), relatively high dielectric breakdown strength, good thermal stability, good chemical stability, small diffusion coefficient, and extremely good CMOS compatibility. The above properties help to eliminate the drawbacks typical of common dielectric materials while retaining excellent compatibility of the dielectric material with current semiconductor fabrication techniques. Moreover, HfO_2 thin films may be fabricated using some relatively mature methods for fabricating thin films such as ALD (atomic layer deposition), MBE (molecular beam epitaxy), PLD (pulsed laser deposition), CVD (chemical vapor deposition), and RF magnetron sputtering **[2-8]**.

The extraordinary versatility of HfO_2 has led to the wide use of this oxide in many advanced electronic devices such as gate dielectrics of MOSFETs, MIM capacitors, DRAMs, RRAMs, FeRAMs, FeFETs, MEMS, and RF passive devices. Moreover, recent years have seen the rising interest in the study of HfO_2 due to its excellent scalability and ability to possess different functionalities depending on the deposition conditions, crystallographic phase, and interface engineering. Many studies have shown that proper control of deposition parameters, thickness of the film, concentration of oxygen vacancies, residual stress, crystallization behavior, and interface between the dielectric and electrode can significantly affect the structure and electrical properties of the HfO_2 thin films. That is why HfO_2 has become one of the most widely studied dielectric materials for conventional applications and novel electronics **[3–10]**.

Within these applications, the metal–insulator–metal (MIM) capacitors have a very special place due to being one of the basic passive elements used in the current integrated circuits. MIM capacitors are widely used in analog, mixed signal, radio frequency (RF), microwave and high-frequency communications circuits due to their good linearity, high frequency stability, low parasitic resistance, high capacitance density, and BEOL fabrication process compatibility.

Unlike the conventional metal–oxide–semiconductor (MOS) capacitors, MIM capacitors typically show less voltage dependency, fewer parasitics, better quality factors and improved performance at high frequencies. All these features make them suitable for applications like analog-to-digital converters, voltage-controlled oscillators, filters, impedance matching, decoupling circuits, energy storage devices, and RF integrated circuits. With the increase in the integration density and reduction of the working voltage in the semiconductor technology, the need for high-performance MIM capacitors with better dielectrics and long term reliability has greatly increased **[8–13]**.

The electrical behavior of MIM capacitors based on HfO_2 is largely dependent on the inherent dielectric behavior of the insulating film as well as the nature of the dielectric–electrode interface. There have been several reports suggesting that the improvement in dielectric constant, capacitance density, leakage behavior, breakdown field, dielectric losses, and lifetime of the device can be accomplished through appropriate manipulation of the dielectric composition, deposition conditions, dielectric interface, and crystalline structure. The methods such as Al doping, multilayer dielectric design, defect passivation, annealing, and interface engineering have been thoroughly explored for the enhancement of the dielectric behavior of the HfO_2 thin film. Similarly, recent review papers have pointed out that electrode selection, thin-film microstructure, defect behavior, oxygen vacancy, and deposition method altogether govern the electrical performance of HfO_2-based capacitors. It is quite evident from the above discussion that dielectric behavior cannot be explained in terms of the dielectric material alone but is the consequence of an interplay between the dielectric film, electrode material, and processing technique **[9-15]**.

As a result, the interdependence of the microstructure of thin films, their dielectric properties, and the performance of devices based on them has become one of the key problems in electronic devices with HfO_2 layers. Many studies were thus conducted to clarify how deposition methods, material composition, defect engineering, crystallization process, and quality of interfaces affect the electrical properties of HfO_2 thin films. Despite the great achievements in this field, there are still some significant problems connected with thin film morphology, electrical properties controlled by interfaces, and electrode materials which require further investigation. It is necessary for the enhancement of HfO2-based MIM capacitor performance in future electronics, radio-frequency (RF), and energy storage applications.

The electrical properties of the HfO_2 thin film are very much dependent on its microstructure that itself depends a lot on the preparation technique and the associated film growth mechanism. Therefore, the deposition method becomes critical in deciding the density, crystalline structure, grain size, surface morphology, interface quality, and the defect nature in the HfO_2 films, influencing the dielectric behavior of HfO2-based devices. Some of the deposition methods used for preparing the HfO_2 thin films are ALD, MBE, PLD, CVD, and magnetron sputtering. Out of all these methods, RF magnetron sputtering has become quite popular due to some of its attractive features like thickness control, uniformity of deposition, high deposition rate, adhesion, low processing cost, and compatibility with the industrial fabrication process of semiconductors.

Moreover, the process of sputtering offers accurate control over the parameters of film deposition, like the operating pressure, RF power, substrate temperature, and oxygen partial pressure, and therefore makes it possible to vary the structural and electrical properties of the HfO_2 thin films systematically. Several investigations have shown that changes in the sputtering conditions can affect the orientation of crystals, grain size, oxygen vacancies, interface formation, and surface morphology **[16-19]**.

In terms of the many parameters that influence the properties of a dielectric, the surface morphology has been found to be one of the most important because it influences interface uniformity, local electric field distribution, thickness uniformity, and mechanisms of charge transport. The smoother and more uniform the surfaces of thin films are, the lower the trap density at interfaces, lower the electric field concentration, higher the dielectric reliability, and better the electrical stability. On the other hand, the rougher the surface of thin film is, the higher the possibility of local electric field enhancement, which causes an increase in leakage currents, dielectric loss, electrical breakdown, and degradation of capacitor properties. It is therefore essential to characterize the morphology of thin films as an integral part of analysis of high-k dielectrics. Atomic Force Microscopy (AFM) is one of the most efficient techniques that can be used to characterize the surface morphology of a sample on a nanometer scale since it offers precise data on surface roughness, grain size distribution, particle aggregation, and topographic uniformity of the surface.

The electrical properties of HfO_2 thin films depend not only on the morphology but also on the intrinsic defects and interfaces. Oxygen vacancies, grain boundaries, dangling bonds, and dielectric-electrode interface states serve as electrically active defects affecting the processes of charge trapping, dielectric polarization, dielectric relaxation, and conduction. The oxygen vacancies serve as a dual factor in the case of HfO_2 thin films. Though the low concentration of oxygen vacancies can affect the processes of crystallization and dielectric polarization, the high concentration of oxygen vacancies leads to the formation of the defect-assisted conducting channels, increasing the leakage current and dielectric losses and deteriorating the electrical properties of HfO_2 thin films. In the same way, the grain boundaries and interfacial defects act as preferred channels of charge transfer affecting frequency-dependent dielectric properties of thin films. Therefore, the recent works are mostly concentrated on the optimization of defect engineering, interface passivation, and film deposition techniques to reduce the concentration of electrically active defects. It has been shown that electrical properties of HfO_2 capacitors result from the combined effect of composition, defects, and interfaces, rather than dielectric permittivity **[10–15, 20–22]**.

The interface between the electrode and the dielectric is another vital factor controlling the behavior of HfO2 capacitors since the interface controls the charging characteristics, the polarization at the interface, electric field, and long-term electrical stability. The bottom electrode, besides being a source of electrical contact to the thin film capacitor, greatly influences the nucleation process, residual stresses, crystal growth, grain orientation, and defect formation in the dielectric layer. Differences in work function, thermal expansion coefficients, surface energies, and chemical activity between various electrodes may change the microstructure of the interface and, hence, electrical properties of the capacitor. Several recent

studies of HfO_2 based dielectric and ferroelectric structures proved that the selection of appropriate electrodes has a great impact on the dielectric constant, leakage currents, breakdown strength, polarization stability, and reliability of these devices **[23]**. Noble metal electrodes like Pt form stable interfaces with decreased oxidation effect, while Al electrodes are compatible with processing, have low resistivity, and wide applications in IC technologies. Nevertheless, the impact of these electrodes on the electrical properties of sputtered HfO_2 capacitors still needs further study **[7, 12–15]**.

The dielectric properties of HfO_2 thin films can be studied by electrical characterization as it allows one to examine the polarization mechanisms, interface states, dielectric relaxation, and frequency response in the presence of an electric field. In the existing methods for characterization, capacitance-voltage (C–V) and conductance-voltage (G–V) methods are especially useful, as they allow revealing the variations in the capacity for charge storage, dielectric polarization, quality of the interface, and frequency response [24]. It should be noted that C–V and G–V measurements conducted within a broad range of frequencies make it possible to determine several critical dielectric parameters, such as dielectric constant (k), dielectric loss (tan δ), quality factor (Q), capacitance density (C/A), parallel resistance (Rp), equivalent impedance, and energy storage capability. The set of the aforementioned dielectric parameters allows obtaining the overall assessment of the dielectric material performance, which makes it possible to compare capacitor structures quantitatively. As the process of polarization and dielectric relaxation depends significantly on the operating frequency, frequency dependent characterization becomes especially valuable when studying dielectric materials that can be used for RF applications **[4, 8, 13, 23]**.

Whereas there have been many studies on the effect of deposition conditions, defect engineering and electrical characterization in HfO_2 based capacitors, relatively little work has been done to understand how various bottom electrode materials affect both thin-film morphology and dielectric properties at various frequencies when processed under the same conditions. Considering the fact that the bottom electrode dictates the nature of the interface developed in the process of forming the films, the use of different materials in forming the electrodes can affect nucleation, roughness, crystallinity and defects, which will in turn affect capacitance and dielectric loss **[25, 26]**.

In recent years, many scientific works have been focused on the improvement of the electrical characteristics of the HfO_2-based capacitors due to material and interface engineering, deposition process and structural optimization. Many experiments have shown that the improvement of dielectric characteristics can be achieved by controlling the phase, decreasing defect concentration, inhibiting leakage channels, and improving the dielectric-electrode interface. Different methods have been proposed to optimize such parameters as dielectric constant, breakdown field, capacitance density, and reliability; those include Al doping, multilayer structure, oxygen vacancy engineering, thermal annealing, and interface passivation **[27,28]**. At the same time, there have appeared many review papers indicating that the electrical properties of HfO_2 films can not be described by intrinsic dielectric properties only; the electrical properties of HfO_2 films depend on the complex interactions between microstructure, interface chemistry, processing conditions, and electrodes **[29, 30]**. It may be concluded that

both optimizations are necessary to achieve stable electrical properties of HfO_2 based capacitors **[9-18]**.

Much of the research carried out so far has been devoted to the topic of dielectric composition optimization for enhancing capacitor performance. This has been evident from the use of aluminum in hafnium dioxide, which is known to influence the phase formation of the dielectric layer, reduce the leakage current, improve the stability of the dielectric layer, and provide long-term reliability. Similarly, there have been suggestions about the use of multiple layers of dielectrics and graded doping techniques in order to improve the capacitance density while keeping the leakage current at an acceptable level **[31]**. While it is true that these techniques are able to highlight the role of dielectric optimization, the dielectric layer is being optimized through changes in its chemical composition. This means that it becomes hard to determine whether the improvement is due to dielectric optimization or the effect of the electrode material **[15-16]**.

The recent research works have also emphasized the important role played by the design of the electrode in governing the structural and electrical properties of hafnium dioxide thin films. The studies conducted on ferroelectric HfO_2 and $HfZrO_2$ systems have revealed that the bottom electrode plays a crucial role in dictating the crystallization process, residual stress, oxygen vacancy profile, phase stability and polarization behavior **[32-33]**. The variation in the work function, interface energy and thermal expansion properties of the electrodes alters the nucleation process and affects the electrical properties of the dielectric layer. In addition, the annealing properties of the electrode material also affect the interface chemistry, defect generation and electrical endurance. It is evident from these studies that the bottom electrode is not only a passive electrode but also an active element that controls the thin film formation process and dielectric performance **[34].** However, most of these studies have been conducted for ferroelectric HfO_2 and $HfZrO_2$ systems wherein the main aim is to optimize the switching characteristics, remanent polarization and memory performance **[35, 22]**.

Another key area coming to light through recent literature is the increasing use of frequency-dependent electrical characterizations. C-V, G-V, impedance spectroscopy, and dielectric spectroscopy have become necessary for dielectric relaxation, interface polarization, charge trapping, and frequency stability characterization of HfO_2-based structures. It has been shown in previous studies that electrical properties like capacitance, conductance, dielectric constant, dielectric loss, and impedance show high frequency dependence since different types of polarizations become dominant at various time scales **[36]**. Therefore, multi-frequency electrical characterization results in much more information than characterization done at one particular frequency. On the other hand, most of the research works available only include certain electrical parameters or concentrate mainly on leakage current, breakdown phenomena, and polarization. Detailed extraction and comparison of various dielectric properties such as dielectric constant (k), dielectric loss (tan δ), quality factor (Q), capacitance density (C/A), and parallel resistance (Rp) from the same experimental data set are not common, especially for sputtered HfO_2-based dielectric capacitors **[37]**.

Along with electrical measurement, another important aspect of research has emerged which is concerned with the correlation between surface morphology and electrical characteristics of the thin films. Some studies have shown that there is a strong dependence of the morphology parameters on deposition parameters, leading to the change of the grains sizes, surface roughness, crystallinity, and defect density and, as a consequence, to changes in the dielectric characteristics and charging mechanisms **[38]**. The atomic force microscopy has become one of the most frequently used methods of nanoscale surface morphology analysis for HfO_2 thin films. However, despite that both the morphological and electrical characterization is performed in a majority of research works, no correlation between these parameters was introduced in many cases. Thus, the direct effect of the surface morphology on the frequency dependent dielectric characteristics is not sufficiently studied **[39]**.

Despite considerable progress in the field due to the reviewed literature, there are still several key areas that lack research. Most of the current literature is devoted to either ferroelectric HfO_2 compounds, memories, gate dielectrics, memristors, composition engineering of dielectrics, or improving reliability by means of doping and annealing. Research related to dielectric HfO_2 thin film deposition by means of RF magnetron sputtering technique is not abundant; at the same time, experiments with dielectric films produced using different bottom electrodes under identical conditions are even more rare **[40]**. In addition, very few studies use a combination of information about thin-film morphology obtained from AFM measurements with multi-frequency C-V/G-V analysis to examine the effect of the bottom electrode material choice on such characteristics as dielectric constant, loss, quality factor, capacitance density, and parallel resistance in various voltage sweep ranges **[41]**.

These findings indicate a definite area that needs further examination. A study carried out in similar conditions of deposition by varying only the bottom electrode material while keeping the same thickness of HfO_2, deposition method, shape of the top electrode, and test electrical conditions would offer invaluable information regarding the influence of the dielectric-electrode interface on capacitor behavior. This way, it is possible to isolate the influence of the bottom electrode from other fabrication parameters and obtain a better understanding of the effect of the interface on both morphology and electric characteristics. The information gained through such a study should help in the development of efficient HfO_2-based MIM capacitors **[42]**.

Inspired by the above facts, the current research attempts to offer a thorough experimental study into the effect of the material used for the bottom electrode on the morphology and frequency dependent electrical properties of HfO_2 thin film MIM capacitors. In contrast to the past investigations, which have concentrated their efforts mainly on the manipulation of dielectric composition, ferroelectric phase formation, and reliability improvement by means of doping and post-deposition processing, the current study has attempted to keep the same dielectric thickness, deposition parameters, shape of top electrode, and electrical characterization technique, with the only difference being in the type of material used for the bottom electrode **[43]**.

In this regard, thin films of 100 nm thick HfO_2 have been deposited via radio frequency (RF) magnetron sputtering on two different materials used as bottom electrodes, namely, Pt coated Si and Al coated SiO2, and top circular aluminum electrodes are fabricated in order to form MIM capacitors consisting of $Al/HfO_2/Pt$ and $Al/HfO_2/Al$ structures. Since identical processing conditions have been utilized in the fabrication of two different capacitor structures, the variations caused by the process can be minimized and a better comparison of the effects of the bottom electrode on film growth and electrical properties can be obtained. Because of the physical and chemical differences between Pt and Al such as work function, surface energy, oxidization reactions, and interface chemistry, these two different materials will affect the nucleation, microstructure development, defect formation, and interaction between the dielectric and the electrode in film growth **[37]**.

In order to determine the interrelationship between morphology and electrical performance, the synthesized thin film structures were studied using atomic force microscopy (AFM) as a tool for investigating surface morphology and roughness. The data on the development of surface structure at the nanometer scale obtained from the AFM analysis can be considered as a quantification of the grain growth, interface uniformity and defect nucleation. The morphological studies were then linked to electrical characterization to explore whether the morphological variations have an effect on the dielectric performance of the MIM capacitors fabricated. This approach is particularly essential since electrical performance is usually evaluated separately from morphological data **[44]**.

Electrical properties of the two capacitors were analyzed by systematic C-V and G-V measurements performed using a Keithley 4200A-SCS semiconductor parameter analyzer over a broad range of frequencies from 100 kHz to 1 MHz. The frequency dependence of the capacitor performance, along with the effect of electric field applied to it, was studied by means of three different voltage sweep values (±2 V, ±5 V, and ±10 V). Along with typical capacitance and conductance analysis, a number of dielectric parameters such as dielectric constant (k), dielectric loss (tan δ), quality factor (Q), capacitance per unit area (C/A), and parallel resistance (Rp) were obtained **[45]**.

A unique aspect about the current study is that all parameters extracted from the dielectric analysis have been analyzed uniformly at different frequencies and at different voltage sweeps for both Pt- and Al-based MIM capacitor designs. The experiment avoids using a single criterion for electrical analysis; rather, the study employs a combination of morphological and frequency dependent dielectric analysis in order to have a more holistic view of the underlying mechanisms of the capacitors' performance. Such an experimental design allows one to understand how the interplay between interfacial properties, dielectric polarization, and energy dissipation depends on the bottom electrode materials used **[46]**.

The results obtained in this study will be helpful in the optimization of HfO_2-based capacitors for high-frequency and microelectronic devices due to the importance of the choice of the bottom electrode for determining the morphology and electrical characteristics of the thin film. The current study not only provides a comparative analysis of the structures of $Al/HfO_2/Pt$ and $Al/HfO_2/Al$ capacitors but also suggests a new systematic approach involving AFM

morphology and multi-frequency dielectric characterization for the evaluation of sputtered HfO_2 thin films. The results are expected to help in designing and manufacturing high-k MIM capacitors, which are needed for advanced microelectronic devices like analog and mixed-signal devices **[22, 23]**.

2. Experimental Methodology

2.1 Materials and Device Fabrication

Two different metal–insulator–metal (MIM) capacitor structures were fabricated to investigate the influence of bottom electrode material on the morphological and frequency-dependent electrical characteristics of HfO_2 thin films. The first structure consisted of Al/HfO_2/Pt, fabricated on a platinized silicon substrate, while the second structure consisted of Al/HfO_2/Al, fabricated on an Al-coated SiO_2 substrate **[12-13]**.

Prior to thin-film deposition, both the platinized silicon and SiO_2 wafer substrates were cut into small pieces of suitable dimensions. The substrates were subsequently cleaned using a standard solvent-cleaning procedure to remove organic and particulate contaminants. Initially, the substrates were ultrasonically cleaned in acetone, followed by rinsing in isopropyl alcohol (IPA). Finally, the samples were thoroughly rinsed with deionized (DI) water and dried using high-purity nitrogen (N_2) gas to obtain clean and contamination-free surfaces before thin-film deposition **[47]**.

For the fabrication of the Al/HfO_2/Pt MIM capacitor, commercially available 2-inch HfO_2 sputtering target was employed for thin-film deposition using the radio-frequency (RF) magnetron sputtering technique. The platinized silicon substrate served as the bottom electrode, while high-purity argon (Ar) was used as the sputtering gas during the deposition process. A uniform HfO_2 dielectric layer with a thickness of approximately 100 nm was deposited onto the Pt-coated substrate under optimized sputtering conditions **[48, 49]**.

For the fabrication of the Al/HfO_2/Al MIM capacitor, a 300 nm thick aluminum (Al) bottom electrode was first deposited onto the cleaned SiO_2 substrate using a thermal evaporation system. Subsequently, a 100 nm HfO_2 dielectric layer was deposited over the Al-coated substrate by RF magnetron sputtering under the same deposition conditions used for the Pt-based sample. During the deposition process, a small portion of the bottom Al layer was intentionally left uncovered to facilitate electrical contact during subsequent electrical measurements **[50]**.

After deposition of the dielectric layer, circular aluminum top electrodes were fabricated on both capacitor structures using a shadow mask-assisted thermal evaporation technique. The top electrodes possessed a diameter of 500 μm of thickness 300 nm, while the center-to-center spacing between adjacent electrodes was maintained at 600 μm. The fabricated device structures were therefore represented as Al/HfO_2/Pt and Al/HfO_2/Al, respectively. A schematic illustration of the fabrication process together with the final device architecture is presented in **(Fig. (1A) & (1B))**.

2.2 Morphological Characterization

The surface morphology of the deposited HfO_2 thin films was examined using Atomic Force Microscopy (AFM) to evaluate the influence of the bottom electrode material on the surface topography of the sputtered dielectric films. AFM analysis was performed to determine the nanoscale surface morphology and to obtain quantitative roughness information. The morphological features that resulted were then related to the electrical properties of the MIM capacitors fabricated to investigate the effect of the thin film microstructure on its dielectric properties **[51]**.

The fabricated MIM capacitors were analyzed using an optical microscope to confirm the presence of the circular top electrodes and the device geometry before electrical testing. Optical micrographs of the fabricated MIM capacitors are shown in **(Fig. (1C) & (1D))**.

2.3 Electrical Characterization

Electrical properties of the fabricated MIM capacitors have been explored through the Keithley 4200A-SCS Semiconductor Parameter Analyzer. C-V and G-V data were collected over three different voltage sweep ranges of −2 V to +2 V, −5 V to +5 V, and −10 V to +10 V. Five separate frequencies of 100 kHz, 200 kHz, 500 kHz, 700 kHz, and 1 MHz were chosen for the study of dielectric behavior of both capacitor designs **[57, 58, 59]**.

In case of $Al/HfO_2/Pt$ capacitors, the electrical measurements were conducted with one probe connected to the circular Al upper electrode and the other one to the Pt lower electrode. On the other hand, for the investigation of electrical properties of $Al/HfO_2/Al$ capacitors, one probe was attached to the circular Al upper electrode, whereas the second probe was placed on the open area of the lower Al electrode which was not covered during the deposition of the dielectric layer **[52]**.

From the C-V and G-V results obtained, some dielectric and electrical characteristics have been derived. The derived characteristics include capacitance (C), conductance (G), dielectric constant (k), dielectric loss ($\tan \delta$), quality factor (Q), capacitance per unit area (C/A), and parallel resistance (Rp). The obtained electrical characteristics have been studied as functions of frequency and voltage sweep to determine the effect of the material of the bottom electrode on the electrical characteristics of the sputtered HfO_2 MIM capacitors.

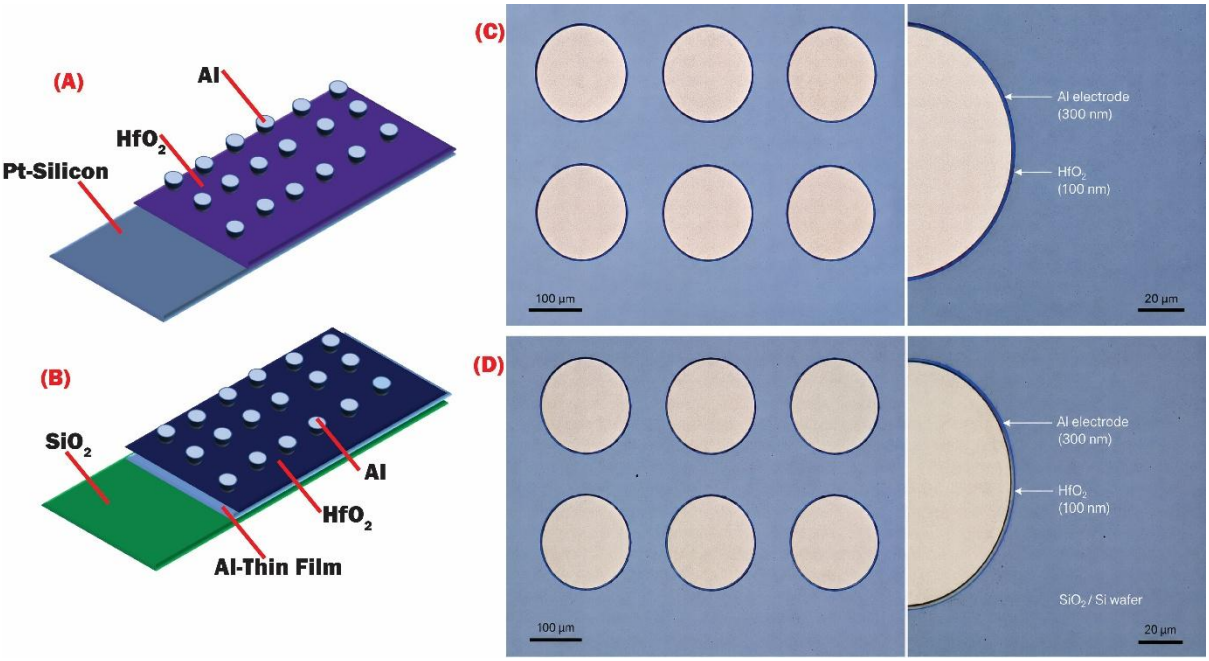


Fig. 1. Schematic illustration of the fabricated HfO_2-based MIM capacitor structures and their corresponding optical microscope images. **(A)** Schematic of the Al/HfO_2/Pt capacitor fabricated by depositing a 100 nm HfO_2 dielectric layer on a platinized Si substrate, followed by a 300 nm thick circular Al top electrode (500 µm diameter). **(B)** Schematic of the Al/HfO_2/Al capacitor fabricated by depositing a 300 nm thick Al bottom electrode on a SiO_2 substrate, followed by a 100 nm HfO_2 dielectric layer and a 300 nm thick circular Al top electrode (500 µm diameter). **(C)** Optical microscope image of the fabricated Al/HfO_2/Pt capacitor. **(D)** Optical microscope image of the fabricated Al/HfO_2/Al capacitor.

Result and Analysis

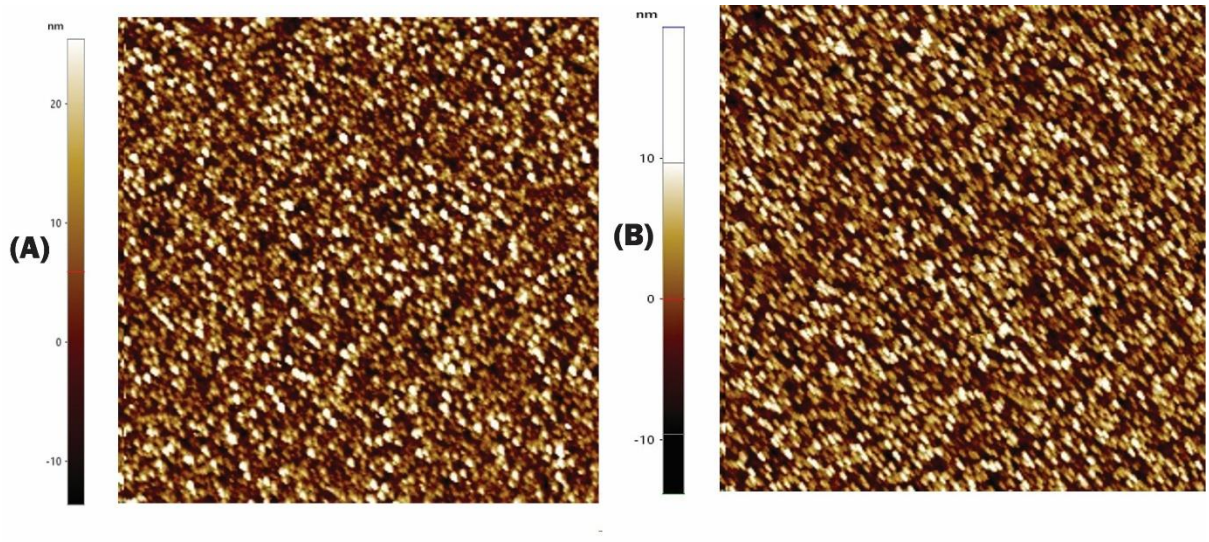


Fig. 2. AFM surface morphology of the sputtered HfO_2 thin films deposited on different bottom electrodes. **(A)** 100 nm HfO_2 thin film deposited on a platinized Si substrate (Pt/HfO_2). **(B)** 100 nm HfO_2 thin film deposited on a 300 nm Al-coated SiO_2 substrate ($Al/HfO_2/Al$).

Fig. 2 shows the AFM surface morphology of the 100 nm RF-sputtered HfO_2 thin films deposited on different bottom electrode materials. As shown in **(Fig. 2(A))**, the HfO_2 film deposited on the platinized Si substrate exhibits a uniform and densely distributed granular morphology with a root mean square (RMS) surface roughness of 4.40 nm. In comparison, the HfO_2 film deposited on the Al-coated SiO_2 substrate **(Fig. 2(B))** shows a slightly higher RMS roughness of 4.90 nm, indicating a relatively rougher surface.

The small difference in surface roughness suggests that the bottom electrode influences the nucleation and growth behavior of the sputtered HfO_2 thin film. Nevertheless, both films exhibit smooth and homogeneous surfaces without noticeable cracks or large agglomerates, indicating good film quality. Such low RMS roughness is desirable for MIM capacitor fabrication because it promotes a uniform dielectric–electrode interface, reduces local electric-field concentration, minimizes interface-related defects, and contributes to stable frequency-dependent electrical characteristics. Therefore, both HfO_2 films are suitable for reliable dielectric layer formation, while the slightly smoother HfO_2/Pt surface is expected to provide a more uniform interface for capacitor operation **[53, 8, 10]**.

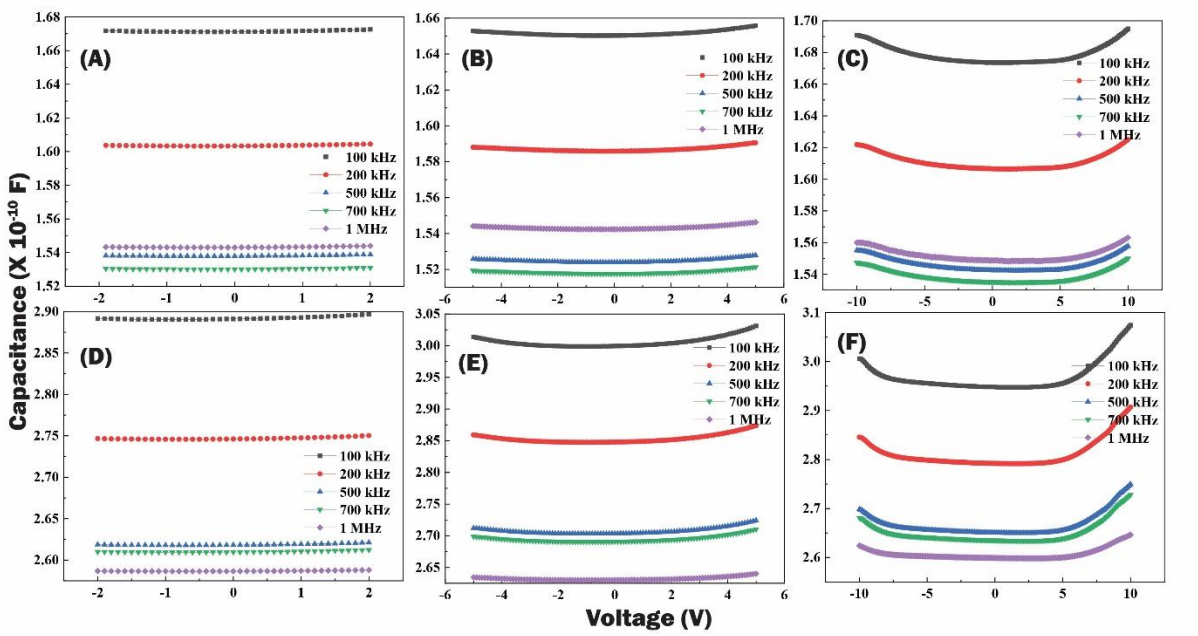


Fig. 3. Frequency-dependent capacitance–voltage (C–V) characteristics of the fabricated MIM capacitors. Panels **(A)–(C)** correspond to the Al/HfO_2/Pt structure measured over voltage sweep ranges of −2 to +2 V, −5 to +5 V, and −10 to +10 V, respectively, while panels **(D)–(F)** show the corresponding C–V characteristics of the Al/HfO_2/Al structure under identical measurement conditions.

Fig. 3. presents the frequency-dependent C–V characteristics of the fabricated Al/HfO_2/Pt and Al/HfO_2/Al MIM capacitors measured under voltage sweep ranges of ±2 V, ±5 V, and ±10 V. For both capacitor structures, the capacitance decreases progressively with increasing measurement frequency from 100 kHz to 1 MHz, indicating the typical frequency dispersion of the HfO_2 dielectric. This behavior can be attributed to the reduced contribution of interfacial and dipolar polarization at higher frequencies, where the polarization mechanisms cannot fully respond to the rapidly varying AC electric field **[54]**.

In the case of the ±2 V sweep range **(Figs. 3(A) & 3(D))**, the value of the capacitance does not change during the voltage sweep, which means there is no voltage dependence in this case due to low electric field strength. In the cases of the increased sweep ranges ±5 V and ±10 V **(Figs. 3(B), 3(C), 3(E), & 3(F))**, the presence of a shallow U-shaped C–V curve with slightly increased capacitance at higher positive and negative bias voltages is observed **[33-34]**.

It can be concluded that the polarization effect occurs under high electric field strength along with a relatively small contribution of the interface charge displacement effects. A comparison of two device structures also shows that Al/HfO_2/Al capacitor possesses significantly higher values of the capacitance than the Al/HfO_2/Pt capacitor for all frequencies. This is related to the influence of the dielectric-electrode interface properties dependent on the bottom electrode type **[55]**.

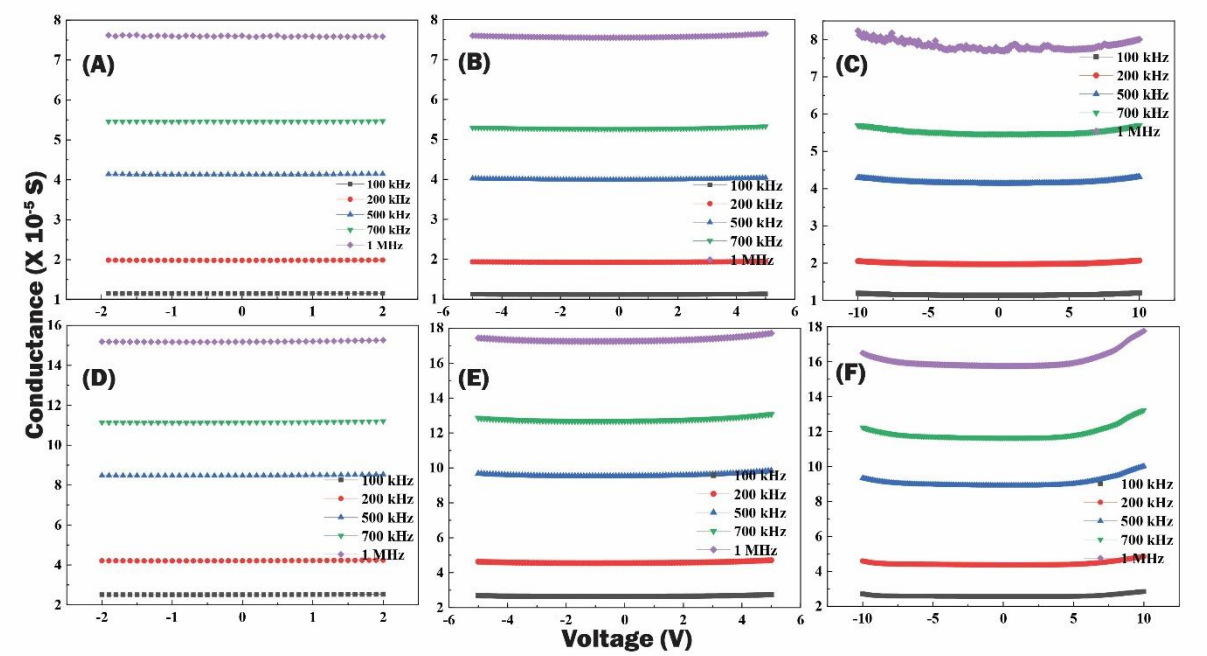


Fig. 4. Frequency-dependent conductance–voltage (G–V) characteristics of the fabricated Al/HfO_2/Pt and Al/HfO_2/Al MIM capacitors measured at 100 kHz, 200 kHz, 500 kHz, 700 kHz, and 1 MHz. Panels **(A)–(C)** correspond to the Al/HfO_2/Pt capacitor measured over voltage sweep ranges of −2 to +2 V, −5 to +5 V, and −10 to +10 V, respectively, whereas panels **(D)–(F)** show the corresponding G–V characteristics of the Al/HfO_2/Al capacitor under identical measurement conditions.

The conductance–voltage (G-V) behavior for frequency dependence of the fabricated Al/HfO_2/Pt and Al/HfO_2/Al MIM capacitors at different sweep ranges of ±2 V, ±5 V, and ±10 V is shown in **(Fig. 4)** at different frequency ranges from 100 kHz to 1 MHz. In case of both the capacitor structures, there is an increase in conductance with the increase in measurement frequency because of the increased AC conduction related to the dielectric material. For the fabricated Al/HfO_2/Pt capacitor, the conductance is increased from about 1.2×10^{-5} S at 100 kHz to about 7.6×10^{-5} S at 1 MHz for the sweep range of ±2 V **[56]**.

With ±2 V sweep **(see Figs. 4(A) & 4(D))**, the conductance stays almost constant over the whole applied bias voltage range, indicating stable conduction and no voltage dependency with relative low electric field strength. In case when the applied voltage sweep is increased to ±5 V and ±10 V **(Figs. 4(B), 4(C), 4(E) & 4(F))**, a shallow "U" shaped conductance curve is observed where there is an increase in the value of the conductance with increasing positive and negative bias voltage **[57]**.

Another comparative analysis of the two structures also shows that in general, the Al/HfO_2/Al configuration always has higher conductance values when compared to the Al/HfO_2/Pt one across the whole range of the frequencies and voltages analyzed. Such a trend is explained by the fact that the conductance values depend not only on the frequency but also on the effect of the electrode at the bottom on the dielectric-electrode interface that leads to the processes of charge movement and interfacial polarization in the sputtered layer of HfO_2. The relatively higher conductance of the Al-bottom-electrode device indicates the increase of the interfacial

conduction and dielectric losses, while the Pt-bottom-electrode device demonstrates the lower conductance values due to its more resistive dielectric interface and AC losses **[58]**.

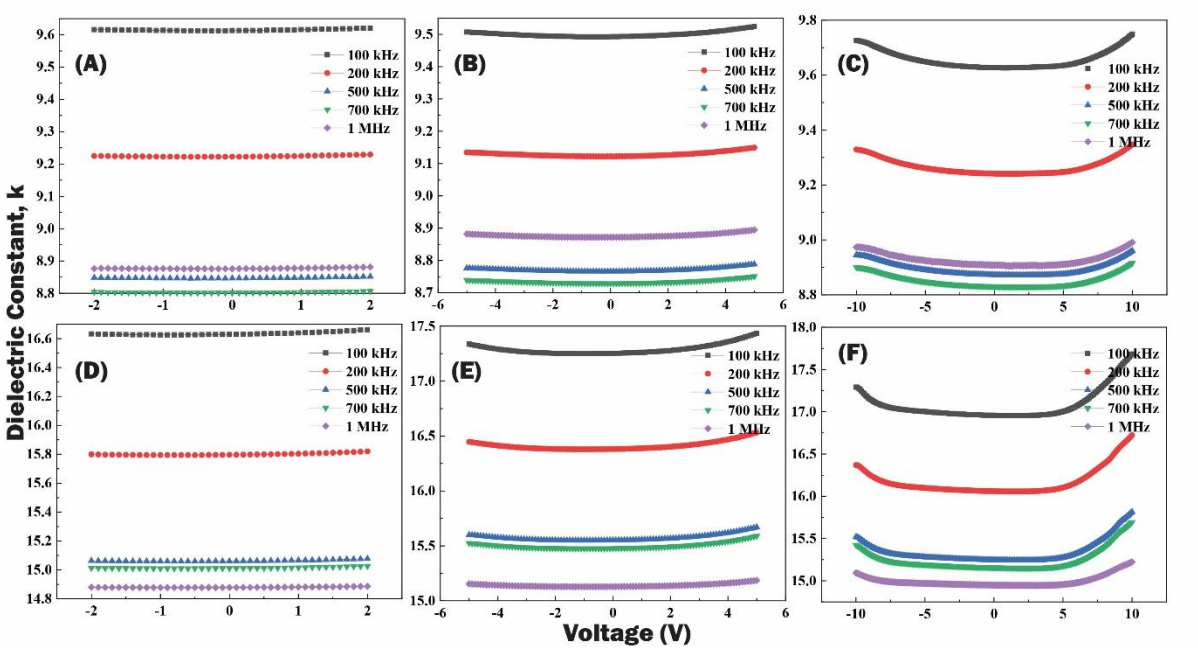


Fig. 5. Frequency-dependent variation of the dielectric constant (k) of the fabricated Al/HfO_2/Pt and Al/HfO_2/Al MIM capacitors measured at 100 kHz, 200 kHz, 500 kHz, 700 kHz, and 1 MHz. Panels **(A)–(C)** correspond to the Al/HfO_2/Pt capacitor extracted over voltage sweep ranges of −2 to +2 V, −5 to +5 V, and −10 to +10 V, respectively, whereas panels **(D)–(F)** show the corresponding dielectric constant characteristics of the Al/HfO_2/Al capacitor under identical measurement conditions.

Fig. 5 represents the variation of the dielectric constant (k) of the developed Al/HfO_2/Pt and Al/HfO_2/Al MIM capacitors with respect to voltage at different frequencies, from 100 kHz to 1 MHz. For both the capacitor designs, the dielectric constant exhibits a gradual fall in value with an increase in frequency, which is a typical property of high-k dielectric materials. The reason behind the decrease in value is that the dipole and interface polarization effects respond very slowly to high-frequency alternating voltage and cannot keep pace with it **[59]**.

With the ±2 V voltage sweep **(see Figs. 5(A) & 5(D))**, the dielectric constant is not dependent on the bias, implying that the dielectric polarization in low electric fields is stable. The Al/HfO_2/Pt capacitor has the dielectric constant of 9.62 at 100 kHz but reduces to 8.83 at 1 MHz. On the other hand, the Al/HfO_2/Al capacitor displays relatively higher dielectric constants, reducing from 16.66 at 100 kHz to 14.89 at 1 MHz. This same trend of behavior is displayed under the ±5 V and ±10 V voltage sweeps **(see Figs. 5(B), 5(C), 5(E), and 5(F))**, where the U-shaped curve shows a minor rise in the dielectric constant with increased positive and negative bias voltages **[60]**.

From the comparison of the two types of capacitor structures, it is quite clear that the Al/HfO_2/Al structure has a much higher value of dielectric constant compared to that of the Al/HfO_2/Pt structure throughout the entire range of frequency and voltage values used in this

experiment. Given that both structures have the same thickness of HfO_2 material and the same deposition process, it can be concluded that the observed differences are mainly due to the effect of the bottom electrode on the interface between the dielectric and the electrode, as well as the effective polarization of the sputtered HfO_2 thin film. The higher value of the dielectric constant observed in the case of the Al-bottom-electrode capacitor suggests better charge polarization and higher effective capacitance, while the Pt-bottom-electrode capacitor displays comparatively low polarization performance **[61]**.

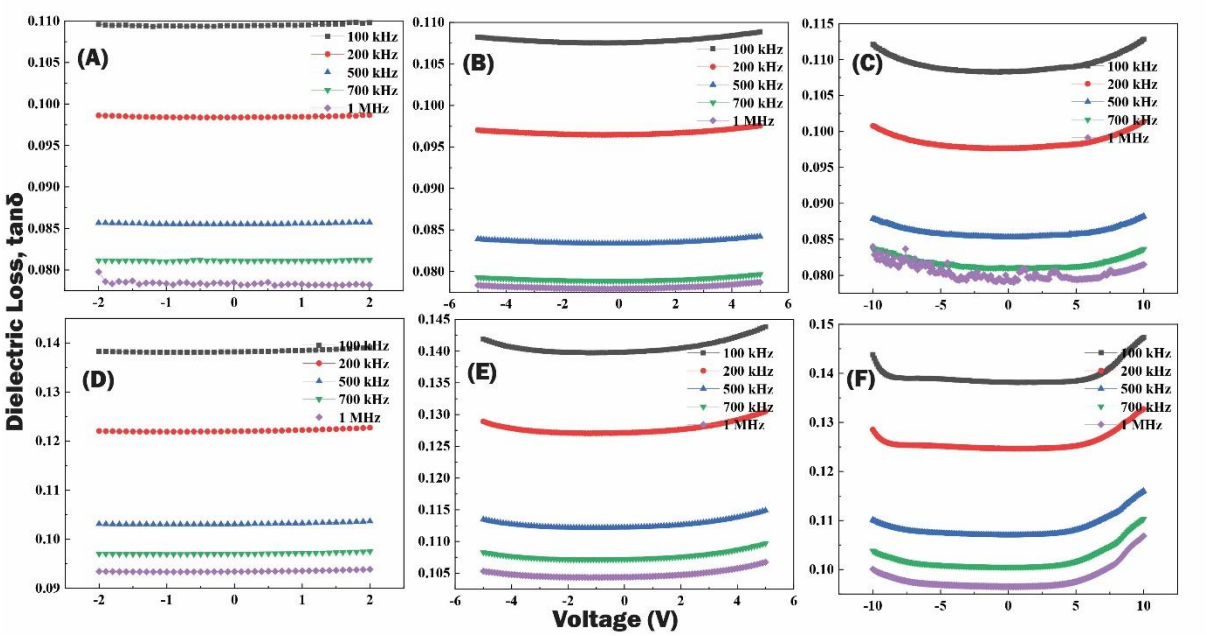


Fig. 6. Frequency-dependent variation of the dielectric loss (tan δ) of the fabricated Al/HfO_2/Pt and Al/HfO_2/Al MIM capacitors measured at 100 kHz, 200 kHz, 500 kHz, 700 kHz, and 1 MHz. Panels **(A)–(C)** correspond to the Al/HfO_2/Pt capacitor extracted over voltage sweep ranges of −2 to +2 V, −5 to +5 V, and −10 to +10 V, respectively, whereas panels **(D)–(F)** show the corresponding dielectric loss (tan δ) characteristics of the Al/HfO_2/Al capacitor under identical measurement conditions.

Fig. 6 presents the variation of the dielectric loss (tan δ) of the fabricated Al/HfO_2/Pt and Al/HfO_2/Al MIM capacitors measured over voltage sweep ranges of ±2 V, ±5 V, and ±10 V at frequencies ranging from 100 kHz to 1 MHz. For both capacitor structures, the dielectric loss decreases progressively with increasing frequency, indicating reduced energy dissipation at higher operating frequencies. This is due to the fact that the interfacial and dipolar polarization processes are hindered, as they cannot keep pace with the rapidly changing electric field at higher frequencies **[62]**.

Under the ±2 V voltage sweep **(Figs. 6(A) & 6(D))**, the dielectric loss is almost constant for all values of the applied voltage, reflecting the stable behavior of the dielectric material at low electric fields. Under the Al/HfO_2/Pt structure, the dielectric loss changes from about 0.109 at 100 kHz to about 0.078 at 1 MHz. The same trend is observed in the case of the Al/HfO_2/Al structure where the dielectric loss reduces from about 0.138 at 100 kHz to about 0.093 at 1 MHz. However, when the sweep voltage increases to ±5 V and ±10 V **(Figs. 6(B), 6(C), 6(E),**

& 6(F)), a shallow U-shape is noticed, with an increase in the dielectric loss at large positive/negative bias voltages **[63]**.

From the above comparison, it can be seen that the Al/HfO_2/Al capacitance system always displays higher dielectric loss compared to the Al/HfO_2/Pt one in the whole range of frequencies and voltages examined. The larger value of the tangent of the loss angle in the case of the Al-bottom-electrode capacitor implies larger dielectric energy losses, which can be caused by more intensive interfacial polarization and charge transportation at the dielectric/electrode interface. On the contrary, smaller dielectric loss found for the Al/HfO_2/Pt capacitor means better dielectric performance with less energy loss at AC mode. Therefore, the influence of the bottom electrode on the dielectric relaxation of the deposited HfO_2 films is evident, and higher frequency of the measurement leads to suppression of dielectric losses **[64]**.

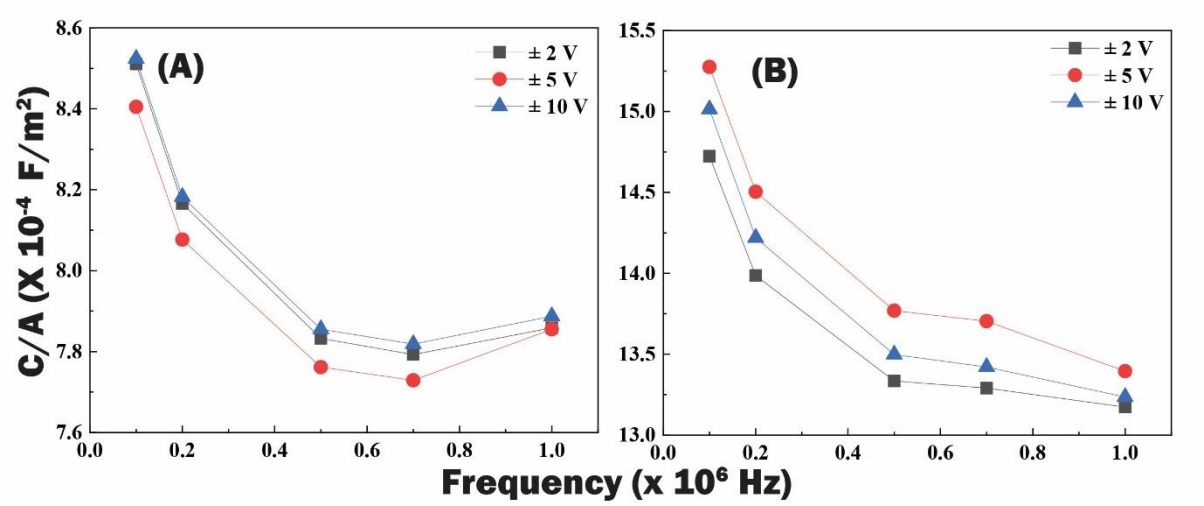


Fig. 7. Frequency dependence of the capacitance density (C/A) of the fabricated Al/HfO_2/Pt and Al/HfO_2/Al MIM capacitors extracted at 0 V bias. Panel **(A)** presents the capacitance density of the Al/HfO_2/Pt capacitor obtained from voltage sweep ranges of −2 to +2 V, −5 to +5 V, and −10 to +10 V, while panel **(B)** shows the corresponding results for the Al/HfO_2/Al capacitor under identical measurement conditions.

As can be seen in **(Fig. 7)**, the frequency dependence of the capacitance density (C/A) of the MIM capacitors with Al/HfO_2/Pt and Al/HfO_2/Al structures fabricated in this study was obtained from 0 V bias in the sweep ranges of ±2 V, ±5 V, and ±10 V. For both types of MIM capacitor, the capacitance density decreases with increase in frequency from 100 kHz to 1 MHz. The decrease in capacitance values at increased frequency corresponds to the reduction in capacitance in the C-V curves **(Fig. 3) [65]**.

In **(Fig. 7(A))**, the capacitance density value of the Al/HfO_2/Pt MIM capacitor decreases from approximately 8.5×10^{-4} F m^{-2} at 100 kHz to about 7.9×10^{-4} F m^{-2} at 1 MHz, while for the Al/HfO_2/Al MIM capacitor **(Fig. 7(B))**, the capacitance density decreases from approximately 15.3×10^{-4} F m^{-2} to 13.2×10^{-4} F m^{-2} over the same frequency range. It can be seen that there are no big changes for ±2 V, ±5 V, and ±10 V sweep ranges; hence, the change in capacitance density is dependent on frequency rather than applied voltage sweep.

In general, the Al/HfO_2/Al MIM structure shows a considerably larger capacitance density compared to the Al/HfO_2/Pt one within the whole tested frequency range, implying a higher charge storage capability. The enhancement is associated with the effect of the bottom electrode on the dielectric-electrode interface, leading to the change in polarization properties of the sputtered HfO_2 thin film. It is seen that the choice of the bottom electrode is an essential factor affecting the capacitance density of HfO_2-based MIM capacitors at high frequencies **[66]**.

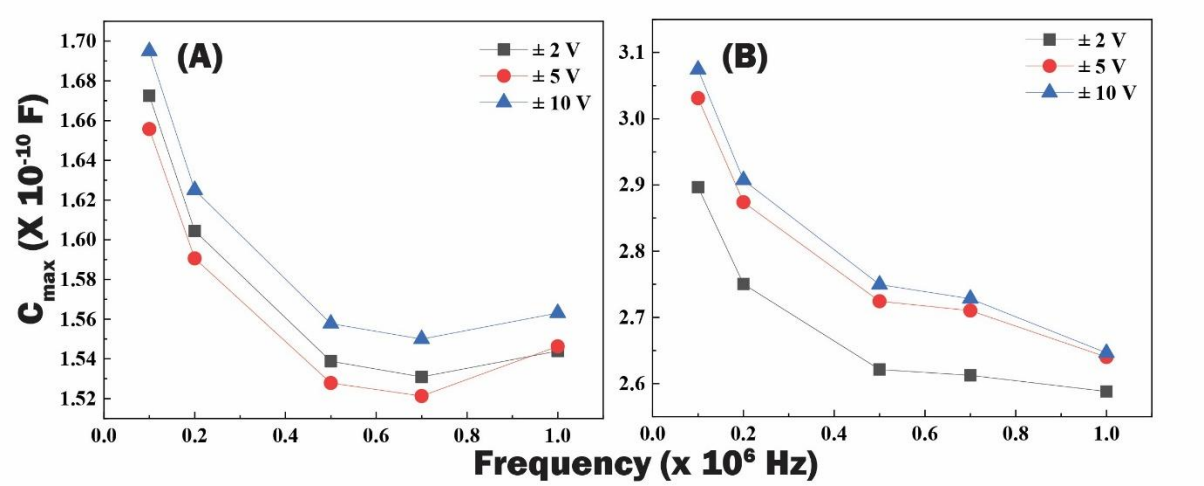


Fig. 8. Comparison of the maximum capacitance (C_{max}) extracted from the C–V characteristics of the fabricated MIM capacitors under different voltage sweep ranges. Panels **(A)** and **(B)** present the C_{max} values obtained from the Al/HfO_2/Pt and Al/HfO_2/Al capacitor structures, respectively, for voltage sweep ranges of −2 to +2 V, −5 to +5 V, and −10 to +10 V.

Fig. 8 depicts the variation of the maximum capacitance (C_{max}) for the fabricated Al/HfO_2/Pt and Al/HfO_2/Al MIM capacitors based on the C-V curves with respect to the frequency for different sweep voltage values of ±2 V, ±5 V, and ±10 V. In both capacitors, the value of maximum capacitance diminishes with an increase in the frequency, similar to that seen in the C-V plots **(Fig. 3)**. This decrease is due to the decreasing effect of interface and dipolar polarization at high frequencies **[67]**.

In the case of the Al/HfO_2/Pt capacitor (Fig. 8(A)), the value of the maximum capacitance drops from approximately 1.67×10^{-10} F at 100 kHz to 1.54×10^{-10} F at 1 MHz. Likewise, for the Al/HfO_2/Al capacitor **(Fig. 8(B))**, there are increased values of C_{max}, which drop from about 3.08×10^{-10} F to 2.64×10^{-10} F within the same frequency range. The value of C_{max} increases slightly when the voltage sweep increases from ±2 V to ±10 V.

In addition to that, the Al/HfO_2/Al capacitor is always shown to have much higher values of maximum capacitance than the Al/HfO_2/Pt capacitor over the whole range of frequencies considered. Taking into account the fact that both capacitors are fabricated from the layers of HfO_2 of the same thickness and under the same deposition conditions, one can conclude that the increased value of C_{max} is due to the effect of the bottom electrode on the dielectric-electrode interface and on the polarization of the HfO_2 dielectric layer **[68]**.

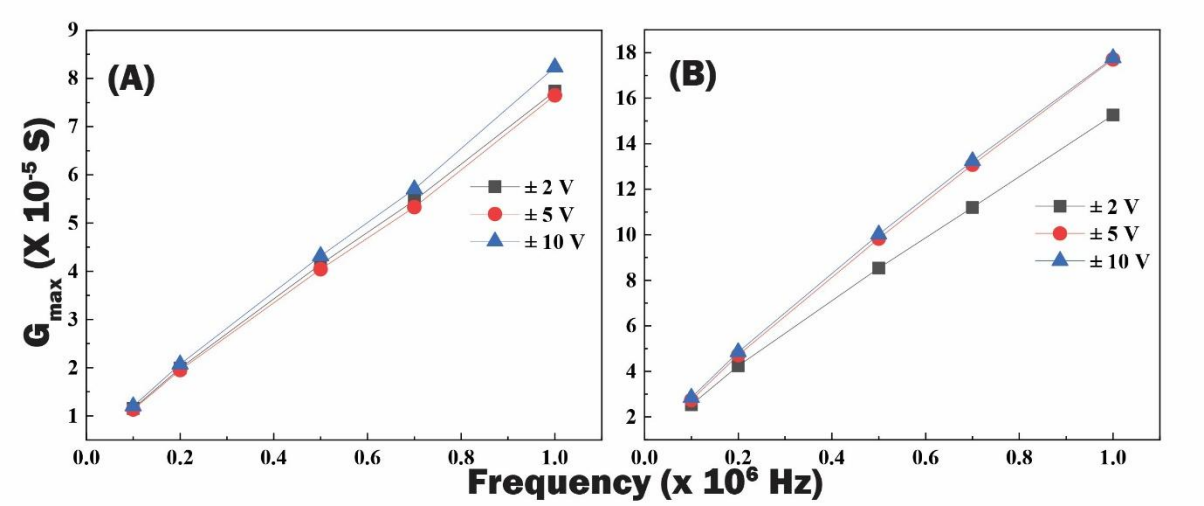


Fig. 9. Maximum conductance (G_{max}) extracted from the measured G–V characteristics of the fabricated Al/HfO_2/Pt and Al/HfO_2/Al MIM capacitors. Panels **(A)** and **(B)** compare the G_{max} values obtained for voltage sweep ranges of −2 to +2 V, −5 to +5 V, and −10 to +10 V, respectively.

Comparison between the maximum conductance (G_{max}) derived from the G-V characteristics of the fabricated Al/HfO_2/Pt and Al/HfO_2/Al MIM capacitors plotted against the frequency is illustrated in **(Fig. 9)** for the voltage sweep values of ±2 V, ±5 V, and ±10 V. Unlike the capacitance variation, the maximum conductance increases nearly linearly with the increasing frequency of measurements for both types of capacitors. This implies an increase in AC conduction as a result of the increased effect of the charge carriers and dielectric relaxation in the HfO_2 film **[55, 56]**.

With regard to the Al/HfO_2/Pt device **(Fig. 9(A))**, the maximum conductance rises from about 1.1×10^{-5} S at 100 kHz to around 8.2×10^{-5} S at 1 MHz. The same trend is observed for the Al/HfO_2/Al capacitor **(Fig. (9B))**, where the maximum conductance rises from about 2.6×10^{-5} S at 100 kHz to about 17.8×10^{-5} S at 1 MHz. There is also a very small rise in G_{max} upon increasing the voltage sweeping from ±2 V to ±10 V.

Additionally, the Al/HfO_2/Al capacitor is seen to display much higher maximum conductance compared to the Al/HfO_2/Pt capacitor within the studied frequency range. As the two types of capacitors have similar thicknesses of HfO_2 and were deposited in similar conditions, the difference is explained by the effects of the bottom electrodes on the dielectric-electrode interface and thus on the charge carriers' transport and dielectric relaxation processes. The high value of G_{max} for the capacitor with an Al bottom electrode is indicative of enhanced AC conductivity and dielectric losses, while the Pt-bottom-electrode capacitor demonstrates lower conductance due to lower losses. This is consistent with the trends observed in the results in **(Fig. 4)** and confirms that the bottom electrode material influences the AC conduction properties of MIM capacitors with sputtered HfO_2 dielectrics **[69]**.

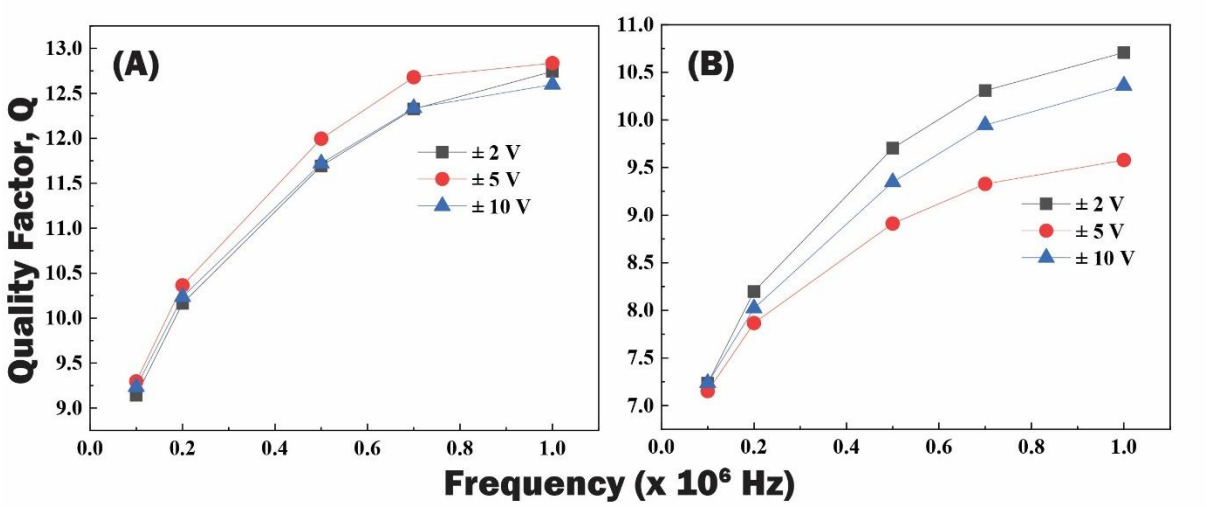


Fig. 10. Frequency dependence of the quality factor (Q) of the fabricated Al/HfO_2/Pt and Al/HfO_2/Al MIM capacitors extracted at 0 V bias. Panels **(A)** and **(B)** show the quality factor of the Al/HfO_2/Pt and Al/HfO_2/Al capacitor structures, respectively, obtained from voltage sweep ranges of −2 to +2 V, −5 to +5 V, and −10 to +10 V.

The variations of the quality factor (Q) of the Al/HfO_2/Pt and Al/HfO_2/Al MIM capacitors are shown in Fig. 10 as a function of frequency at 0 V bias for different voltage sweep intervals of ±2 V, ±5 V, and ±10 V. In both cases, the value of the quality factor increases progressively with increasing frequency of measurement, which can be correlated to the decreasing dielectric losses (see Fig. 6). As the quality factor is directly proportional to the inverse of the dielectric loss, the increase in Q shows better dielectric behavior at higher frequencies **[65, 67, 70]**.

In case of the Al/HfO_2/Pt structure, as seen from **(Fig. 10(A))**, the quality factor is increased from roughly 9.2 at 100 kHz to almost 12.8 at 1 MHz. Similarly, the increase in the quality factor of the Al/HfO_2/Al structure, as shown in **(Fig. 10(B))**, is from about 7.2 at 100 kHz to almost 10.7 at 1 MHz. There are some minor differences noticed for the three different voltage sweeps, namely ±2 V, ±5 V, and ±10 V, but the frequency variation is mostly similar, suggesting that the quality factor depends more on frequency than voltage sweeps **[22, 23]**.

The difference between these two types of capacitors shows that the Al/HfO_2/Pt capacitor always demonstrates a higher value of the quality factor compared to the Al/HfO_2/Al capacitor in the whole frequency range considered. It is because the dielectric loss is rather low in the case of the Pt-bottom-electrode, which is also characterized by the low level of AC conduction, so that the energy storage and power dissipation processes are performed in a more effective way. At the same time, the comparatively low Q factors observed in the case of the Al/HfO_2/Al capacitor correspond to the increased dielectric loss and conductivity **[25, 26]**.

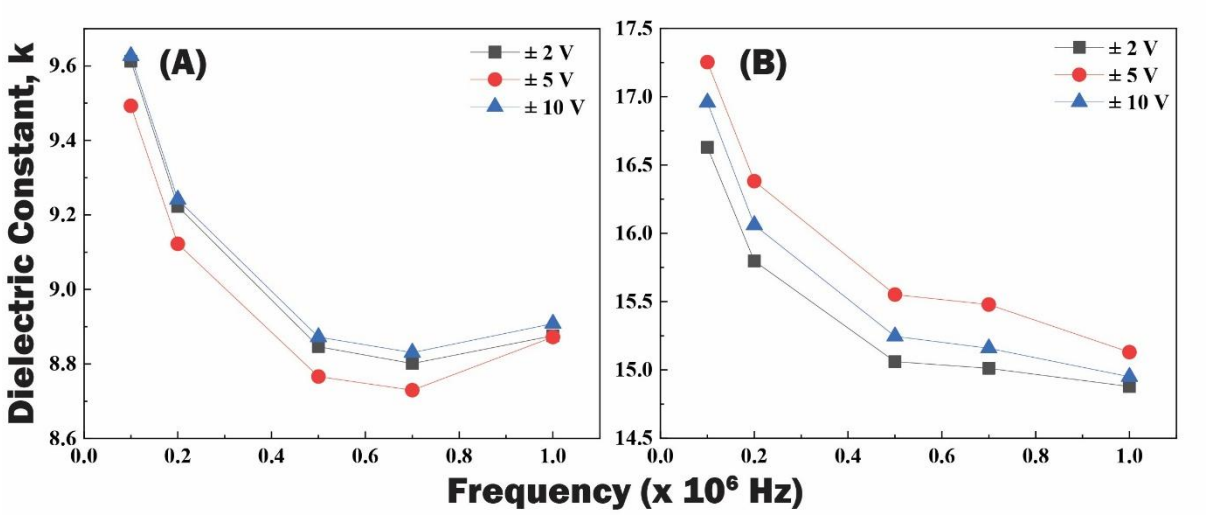


Fig. 11. Frequency dependence of the extracted dielectric constant (k) at 0 V bias for the fabricated Al/HfO_2/Pt and Al/HfO_2/Al MIM capacitors. Panels **(A)** and **(B)** show the dielectric constant of the Al/HfO_2/Pt and Al/HfO_2/Al capacitor structures, respectively, obtained from voltage sweep ranges of −2 to +2 V, −5 to +5 V, and −10 to +10 V.

The dielectric constant (k) of the Al/HfO_2/Pt and Al/HfO_2/Al MIM capacitors has been compared in **(Fig. 11)** as a function of frequency at 0 V bias, while the range of voltage sweep was ±2 V, ±5 V, and ±10 V. For both capacitor types, it has been observed that the dielectric constant reduces with increase in frequency ranging from 100 kHz to 1 MHz due to the usual frequency dispersion in the HfO_2 dielectric. This is because of the gradual reduction of the effect of interfacial and dipole polarization at higher frequencies due to their inability to respond to the changing electric field **[27, 28, 29-30]**.

Regarding the case of Al/HfO_2/Pt capacitor **(Fig. 11(A))**, there is a reduction in the dielectric constant value from 9.62 (at 100 kHz) to 8.89 (at 1 MHz). Similarly, Al/HfO_2/Al capacitor **(Fig. 11(B))** also demonstrates a reduction from 17.2 to 14.9 across the same range of frequency. There are small variations in the dielectric constant value from the three ranges of voltage sweeps (±2 V, ±5 V, and ±10 V), implying that the extracted k values for zero-bias operation are not significantly affected by voltage sweep but depend on the frequency of measurement **[70]**.

It is observed that the dielectric constant of Al/HfO_2/Al capacitor is substantially larger compared to the Al/HfO_2/Pt capacitor across the whole range of measured frequencies. As the same thickness of HfO_2 layer was used in both the devices under the same deposition process, this increase can be attributed to the influence of the interface effect between the dielectric and the bottom electrodes due to different materials. This is in agreement with the dielectric constant dependence on voltage sweep shown in Fig. 5, and proves that bottom electrode manipulation can serve as an efficient way to engineer the dielectric properties of sputtered HfO_2 based MIM capacitors **[71]**.

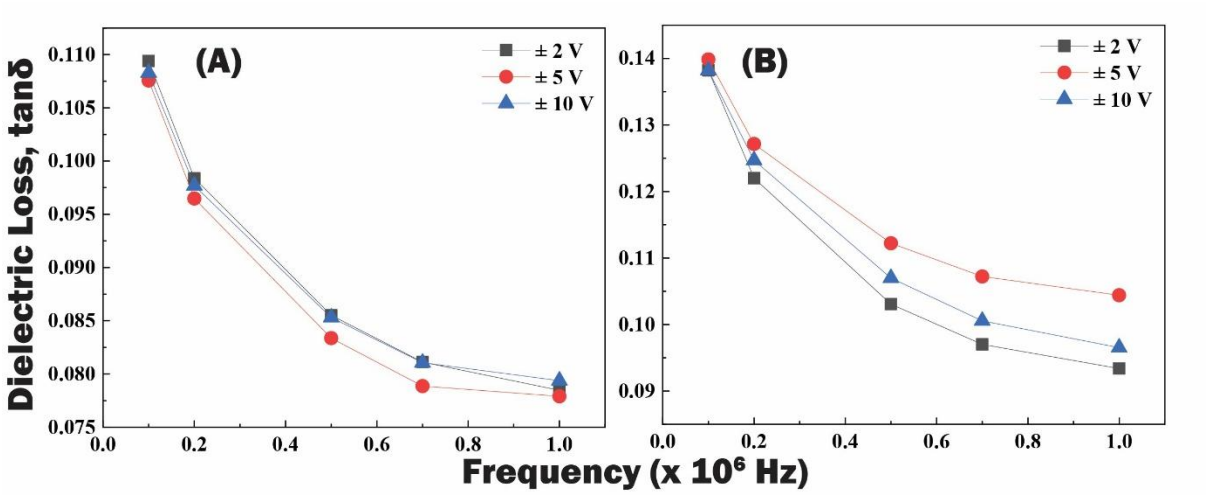


Fig. 12. Frequency dependence of the extracted dielectric loss (tan δ) at 0 V bias for the fabricated Al/HfO_2/Pt and Al/HfO_2/Al MIM capacitors. Panels **(A)** and **(B)** compare the dielectric loss values extracted from voltage sweep ranges of −2 to +2 V, −5 to +5 V, and −10 to +10 V, respectively.

Fig. 12 presents the frequency dependence of the dielectric loss (tan δ) of the fabricated Al/HfO_2/Pt and Al/HfO_2/Al MIM capacitors extracted at 0 V bias for voltage sweep ranges of ±2 V, ±5 V, and ±10 V. For both capacitor structures, the dielectric loss decreases continuously with increasing frequency from 100 kHz to 1 MHz, indicating a reduction in dielectric energy dissipation at higher operating frequencies. This is due to the reduced role of interfacial and dipole polarization, since they cannot react to the alternating electric field fast enough due to their nature **[55, 56]**.

In the case of the Al/HfO2/Pt capacitor **(Fig. 12(A))**, there is a reduction in dielectric loss from around 0.109 at 100 kHz to around 0.079 at 1 MHz. In addition, the Al/HfO_2/Al capacitor **(Fig. 12(B))** also shows a reduction in dielectric loss from about 0.140 to 0.094. The dielectric losses obtained from all three voltage sweep cases (±2V, ±5V, and ±10V) show a close match, implying that dielectric loss measured at 0V bias is not significantly affected by the voltage sweep range but depends mostly on the measurement frequency **[71]**.

In addition, it can be noted that the Al/HfO_2/Pt capacitor shows the lowest values of dielectric loss in comparison with the Al/HfO_2/Al capacitor in the whole examined frequency range, which indicates the lowest energy losses in such case. On the contrary, the rather higher tan δ of the Al/HfO_2/Al capacitor can be explained by the higher degree of dielectric relaxation and interfacial losses related to the use of Al as the bottom electrode. The obtained experimental results are well-correlated with the data on voltage-dependent dielectric losses of the capacitor **(Fig. 6)** and quality factor analysis **(Fig. 10)**, which is due to the higher value of quality factor in the case of the Al/HfO_2/Pt capacitor because of its lower dielectric losses **[72]**.

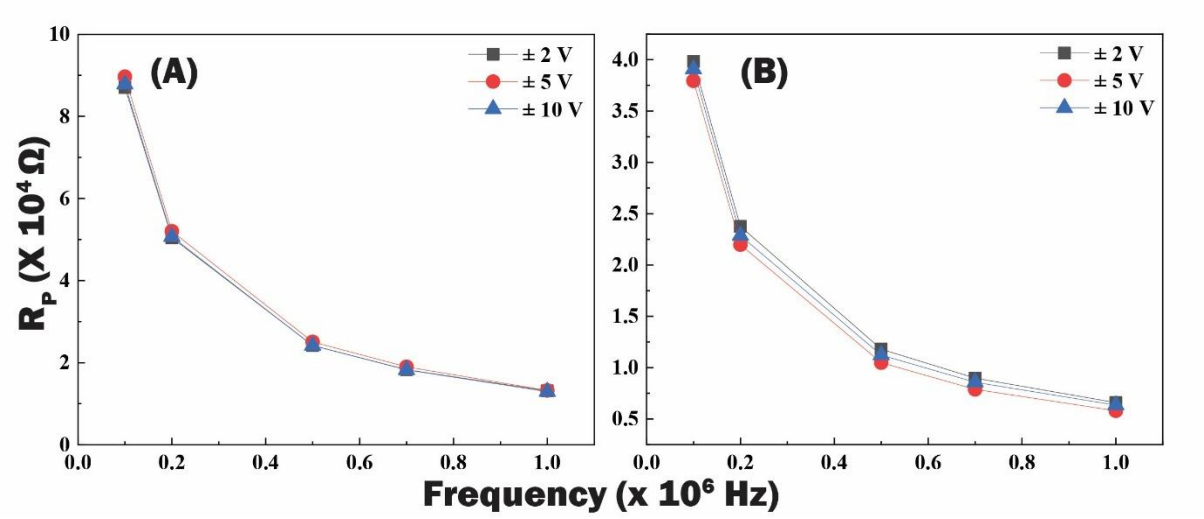


Fig. 13. Frequency dependence of the extracted parallel resistance (R_p) at 0 V bias for the fabricated Al/HfO_2/Pt and Al/HfO_2/Al MIM capacitors. Panels **(A)** and **(B)** compare the parallel resistance values extracted from voltage sweep ranges of −2 to +2 V, −5 to +5 V, and −10 to +10 V, respectively.

Fig. 13 presents the variation of the extracted parallel resistance (R_p) of the fabricated Al/HfO_2/Pt and Al/HfO_2/Al MIM capacitors as a function of frequency at 0 V bias for voltage sweep ranges of ±2 V, ±5 V, and ±10 V. For both capacitor structures, the parallel resistance decreases continuously with increasing frequency from 100 kHz to 1 MHz, indicating an increase in AC conduction and a reduction in the effective resistive impedance of the dielectric layer at higher operating frequencies. This behavior is consistent with the increase in conductance **(Fig. 9)** and reflects the enhanced response of charge carriers under high-frequency excitation **[63, 72]**.

For the Al/HfO_2/Pt capacitor **(Fig. 13(A))**, the parallel resistance decreases from approximately 8.9×10^4 Ω at 100 kHz to about 1.3×10^4 Ω at 1 MHz. Similarly, the Al/HfO_2/Al capacitor **(Fig. 13(B))** exhibits lower resistance values, decreasing from approximately 4.0×10^4 Ω to 0.65×10^4 Ω over the same frequency range. The values obtained from the three voltage sweep conditions (±2 V, ±5 V, and ±10 V) are very close to each other, indicating that the extracted R_p at 0 V bias is only marginally affected by the voltage sweep range and is predominantly governed by the measurement frequency **[12, 14]**.

A comparison between the two capacitor structures clearly shows that the Al/HfO_2/Pt capacitor exhibits consistently higher parallel resistance than the Al/HfO_2/Al capacitor throughout the investigated frequency range. The higher R_p of the Pt-bottom-electrode device indicates lower leakage conduction, improved dielectric insulation, and reduced energy dissipation, whereas the lower R_p observed for the Al-bottom-electrode device suggests comparatively higher conductive losses at the dielectric–electrode interface. These observations are in excellent agreement with the previously discussed conductance **(Fig. 9)**, dielectric loss **(Fig. 12)**, and

quality factor **(Fig. 10)** results, where the Pt-based capacitor exhibited lower conductance, lower dielectric loss, and higher quality factor. Overall, the results demonstrate that the bottom electrode material plays a significant role in determining the resistive behavior and dielectric insulation quality of sputtered HfO_2-based MIM capacitors, with the Al/HfO_2/Pt structure exhibiting superior electrical insulation characteristics for high-frequency capacitor applications **[73, 74]**.

6. Conclusion

In this work, the influence of bottom electrode material on the morphological and frequency-dependent electrical characteristics of RF-sputtered HfO_2 thin-film MIM capacitors was systematically investigated by comparing Al/HfO_2/Pt and Al/HfO_2/Al capacitor structures fabricated under identical deposition conditions. AFM analysis confirmed the successful deposition of uniform HfO_2 thin films on both substrates, with RMS surface roughness values of 4.40 nm for the Pt-based structure and 4.90 nm for the Al-based structure, indicating good surface quality suitable for dielectric capacitor applications.

Electrical characterization performed over the frequency range of 100 kHz–1 MHz and voltage sweep ranges of ±2 V, ±5 V, and ±10 V revealed that both capacitor structures exhibited stable frequency-dependent dielectric behavior. The capacitance, dielectric constant, and capacitance density were observed to decrease with an increase in frequency, while the conductance was observed to increase with the increase in frequency, which is the characteristic behavior associated with the dielectric relaxation of HfO_2 thin films.

Comparison of the two device configurations confirmed that the Al/HfO_2/Al capacitor had always shown higher values of capacitance, dielectric constant, capacitance density, and conductance; thus, the polarization and charge storage were improved. On the contrary, the Al/HfO_2/Pt capacitor had lower dielectric loss, higher quality factor, and higher parallel resistance, thereby indicating lower dielectric losses, better electrical insulation, and more energy efficiency. This difference is due to the effect of the material of the bottom electrode at the dielectric-electrode interface affecting the polarization and charge transport in the sputtered HfO_2 dielectric layer.

In general, this investigation proves that bottom electrode engineering can serve as a useful strategy for the manipulation of electrical characteristics of sputtered HfO_2 thin-film MIM capacitors without changing the properties of the dielectric and the method of its fabrication. Though the Al/HfO_2/Al configuration is more appropriate for high capacitance density and charge retention applications, the Al/HfO_2/Pt configuration can be considered as a better option due to its superior dielectric insulation, lower energy losses and higher Q-factor, which makes it a good choice for RF capacitor applications.

CRediT authorship contribution statement

Abdullah: Conceptualization, Methodology, Investigation, Formal analysis, Data curation, Validation, Visualization, Writing – original draft, Writing – review & editing, Resources.

Declaration of competing interest

The author declares that there are no known competing financial interests or personal relationships that could have appeared to influence the work reported in this paper.

Acknowledgement

The authors thank Prof. Mahesh Kumar and the Central Research Facility (CRF), IIT Jodhpur, for providing access to the facilities and instruments used in this research.

Data availability. Data will be made available on request.

References

[1] C. Fohn, E. Chery, K. Croes, M. Stucchi, V. Afanas'ev, Multi-step trap-assisted tunneling in Al-doped HfO_2 used in advanced 2.5D metal–insulator–metal capacitors, *J. Appl. Phys.* **138** (2025) 074104. https://doi.org/10.1063/5.0277092

[2] B. Cao, Y. Duan, L. Shao, Modeling and characterization of thin Al_2O_3–HfO_2 stacked metal–insulator–metal and deep trench decoupling capacitors for advanced packaging applications, *J. Phys.: Conf. Ser.* **3223** (2026) 012011. https://doi.org/10.1088/1742-6596/3223/1/012011

[3] H.-F. Shiue, C.-H. Chuang, C.-L. Mo, M.-J. Chen, Dramatic leakage current suppression in HfO_2 gate dielectrics via atomic layer hydrogen manipulation, *Mater. Sci. Semicond. Process.* **193** (2025) 109859. https://doi.org/10.1016/j.mssp.2025.109859

[4] D. Yadav, H. Levene, S. Stathopoulos, R. Ramesh, S. Kumar, T. Prodromakis, Impedance spectroscopy of hafnium oxide: Memristive and memcapacitive switching with annealing, *IEEE Trans. Electron Devices* **72** (5) (2025) 2271–2279.

[5] X. Zhang, S. Chen, M. Sun, M. Gou, H. Ma, Simulation and design of the 3D silicon capacitor structure characterized by low-parasitic, high-capacitance and high-reliability, in: *2025 26th International Conference on Electronic Packaging Technology (ICEPT)*, IEEE, 2025, pp. 1–5. https://doi.org/10.1109/ICEPT67137.2025.11157335

[6] Y. Nam, T. Kwak, H. Ma, S. Oh, S. Park, M. Yoon, D. Kyung, G. Yoo, S.-W. Kim, O. Nam, Normally-off Al/HfO_2/Al-gated diamond field effect transistor on a heteroepitaxial diamond substrate, *Diamond Relat. Mater.* **164** (2025) 113258. https://doi.org/10.1016/j.diamond.2025.113258

[7] C. Han, K.R. Kwon, S. Jeong, B. Kwak, J. Yim, E.C. Park, J.W. You, R. Choi, D. Kwon, Tunable ferroelectric properties of HfO_2-based oxides: Role of aluminum doping and bottom electrodes, *IEEE Trans. Electron Devices* **72** (2) (2025) 635–643. https://doi.org/10.1109/TED.2024.3517593

[8] H. Park, C. Han, Y. Choi, M. Choi, S. Won, C. Shin, Effect of bottom electrode annealing temperature and atmosphere on endurance characteristics of ferroelectric $Hf_{0.5}Zr_{0.5}O_2$ capacitors, *IEEE Electron Device Lett.* **46** (11) (2025) 2038–2041. https://doi.org/10.1109/LED.2025.3603933

[9] E. Kim, J. Woo, Evolution of materials and device stacks for HfO_2-based ferroelectric memories, *Adv. Mater. Interfaces* (2026). https://doi.org/10.1002/admi.202600040

[10] Z. Zhou, L. Li, Y. Feng, X. Wang, Z. Zheng, L. Jiao, H. Zheng, Y. Shi, K.-W. Ang, X. Gong, Advancing the frontiers of HfO_2-based ferroelectric memories: Innovative concepts from materials to applications, *Adv. Mater.* (2025). https://doi.org/10.1002/adma.202507324

[11] S. Lancaster, S. Slesazeck, T. Mikolajick, On the thickness scaling of ferroelectric hafnia, *IEEE Trans. Mater. Electron Devices* **1** (2024) 36–45. https://doi.org/10.1109/TMED.2024.3453822

[12] F. Yan, Y. Wu, Y. Liu, P. Ai, S. Liu, S. Deng, K.-H. Xue, Q. Fu, W. Dong, Recent progress on defect-engineering in ferroelectric HfO_2: The next step forward via multiscale structural optimization, *Mater. Horiz.* **11** (2024) 626–645. https://doi.org/10.1039/D3MH01590A

[13] T. Lee, J. Bong, H. Lee, H.-S. Lee, H.-S. Jang, H.-T. Kim, J.-H. Lee, B.J. Cho, Y.-H. Choi, H. Bae, T. Moon, K. Heo, Enhanced dielectric constant by Al gradient doping on atomic-layer-deposited HfO_2-based metal–insulator–metal capacitor, *Adv. Electron. Mater.* (2026). https://doi.org/10.1002/aelm.202501683

[14] T. Dehury, S. Kumar, S. Pütter, S. Roy, S. Sahoo, C. Rath, Volatile resistive switching characteristics of molecular beam epitaxy grown HfO_2 thin films, *Appl. Surf. Sci.* **685** (2025) 162060. https://doi.org/10.1016/j.apsusc.2024.162060

[15] J. Theocharis, J.P. Martins, A. Mahjoub, E. Eustache, A. Ziaei, G. Papaioannou, On the electrical properties of ALD HfO_2 dielectric films for MEMS capacitive switches, *Microelectron. Reliab.* **168** (2025) 115737. https://doi.org/10.1016/j.microrel.2025.11573

[16] E. Chery, K. Croes, P. Nolmans, E. Beyne, Characterization and reliability study of an Al-doped HfO_2-based high-density 2.5-D MIMCAP, *IEEE Trans. Electron Devices* **71** (6) (2024) 3845–3852. https://doi.org/10.1109/TED.2024.3386871

[17] N. Shulaev, A. Bobylev, S. Udovichenko, M. Grigoriev, N. Azarapin, Synthesis and study of Al:HfO_2 thin films for memristors: Structural and properties, in: *2025 IEEE 26th International Conference of Young Professionals in Electron Devices and Materials (EDM)*, IEEE, 2025, pp. 1–5. https://doi.org/10.1109/EDM65517.2025.11096864

[18] C. Fohn, F. Zharfan, E. Chery, K. Croes, M. Stucchi, V. Afanas'ev, Impact of Al-doping on Al:HfO_2 dielectric reliability in MIM capacitors, in: *Proceedings of the IEEE International Reliability Physics Symposium (IRPS)*, IEEE, 2025.

[19] D. Kannadassan, K. Sivasankaran, S. Kumaravel, C.-H. Cheng, M. Shojaei Baghini, P.S. Mallick, High-*k* metal–insulator–metal capacitors for RF and mixed-signal VLSI circuits: Challenges and opportunities, *Proc. IEEE* **113** (1) (2025) 104–138. https://doi.org/10.1109/JPROC.2024.3513326

[20] S. Zhang, C. Wang, D. Li, W. Zhang, X. Huang, J. Zhu, Enhancement of laser-induced damage threshold of HfO_2 thin films via substrate heating during magnetron sputtering, *Appl. Surf. Sci.* **695** (2025) 162853. https://doi.org/10.1016/j.apsusc.2025.162853

[21] T. Onaya, T. Nabatame, Interface engineering of HfO_2-based ferroelectric devices for crystal phase control and enhanced ferroelectricity using atomic-layer-deposited ZrO_2 nucleation layers, *Jpn. J. Appl. Phys.* **65** (2026) 080804. https://doi.org/10.35848/1347-4065/adb6db

[22] S. Strangio, E. Dimaggio, D. Marian, A. Catania, A. Toral-Lopez, F. Pieri, G. Iannaccone, G. Fiori, Advanced materials-based technologies for security and cryptographic applications: Opportunities and challenges, *Adv. Funct. Mater.* (2026). https://doi.org/10.1002/adfm.202601738

[23] F. Yan, Y. Wu, Y. Liu, P. Ai, S. Liu, S. Deng, K.-H. Xue, Q. Fu, W. Dong, Recent progress on defect-engineering in ferroelectric HfO_2: The next step forward via multiscale structural optimization, *Mater. Horiz.* **11** (2024) 626–645. https://doi.org/10.1039/D3MH01590A

[24] D.B. Kastian, Y.-H. Lin, Y.-C. Chen, C.-H. Hsu, C.-C. Kuo, C.-H. Cheng, Influence of bilayer high-*k* Al_2O_3 and HfO_2 gate insulators on the electrical performance of amorphous oxide thin-film transistors, *J. Phys. D: Appl. Phys.* **59** (2026) 045102. https://doi.org/10.1088/1361-6463/ad9d9b

[25] J.Y. Lee, H.-J. Choi, K.H. Ye, H. Choi, B.-H. Lee, M.-S. Kim, D.-H. Han, J.H. Lee, S.O. Won, T.H. Kim, H.J. Chang, J.-H. Choi, S.-H. Baek, Engineering of crystal and domain structures in epitaxial Y:HfO_2 thin films by YSZ substrate miscut, *Adv. Sci.* **13** (2026) 2506076. https://doi.org/10.1002/advs.202506076

[26] J.K. Porala, S. Zhang, W.F. Lim, Temperature-dependent high-*k* HfO_2 gate dielectrics for next generation power devices, *Microelectron. Eng.* **312** (2025) 112024. https://doi.org/10.1016/j.mee.2025.112024

[27] I. Hwang, H. Nam, J. Kim, B. Kim, Y. Jang, W. Lee, M. Kang, C. Yoon, Interface-engineered, low-damage IGZO/HfO_2 charge-trapping memory devices fabricated using a remote plasma ALD process, *Micromachines* **17** (2026) 743. https://doi.org/10.3390/mi17060743

[28] T. Lee, J. Bong, H. Lee, H.-S. Lee, H.-S. Jang, H.-T. Kim, J.-H. Lee, B.J. Cho, Y.-H. Choi, H. Bae, T. Moon, K. Heo, Enhanced dielectric constant by Al gradient doping on atomic-layer-deposited HfO_2-based metal–insulator–metal capacitor, *Adv. Electron. Mater.* (2026) e2500679. https://doi.org/10.1002/aelm.202500679

[29] J. Xu, Y. Cao, R. Kang, Y. Gao, W. Qiao, H. Ci, J. Mei, M. Bai, J. Zhao, Y. Zhao, K. Zeng, X. Lou, Excellent ferroelectricity and thermal stability in Ce-doped HfO_2 thin films via oxygen vacancy modulation, *ACS Appl. Mater. Interfaces* (2026). https://doi.org/10.1021/acsami.6c07990

[30] M.T. Alam, M.A. Hossain, J. Kim, S. Kim, Electrical characterization of high-*k* ($k > 115$) crystalline $SrTiO_3$ (STO) thin film integration with GaN with nanomembrane transfer process, *Semicond. Sci. Technol.* **41** (2026) 055018. https://doi.org/10.1088/1361-6641/ade06f

[31] O. Kaatranen, P. Eskelinen, S. Inkinen, O.-P. Kilpi, K.-M. Persson, Ferroelectric HfO_2/ZrO_2 superlattice capacitors with high center-to-edge wafer-scale uniformity, *Adv. Electron. Mater.* (2026) e2501624. https://doi.org/10.1002/aelm.202500773

[32] Y. Zhang, Z. Lu, Y. Yang, X. Wang, Y. Meng, J. Yue, J. Wang, D. Wang, Y. Sun, W. Li, X. Wang, X. Lu, Machine learning-guided phase-structure design for optimizing the ferroelectric properties of doped HfO_2, *Mater. Sci. Semicond. Process.* **189** (2025) 109678. https://doi.org/10.1016/j.mssp.2025.109678

[33] H. Yu, X. Zhang, H. Cai, L. Pei, Y. Xue, J. Liu, Optimizing the wide-temperature tribological properties of HfO_2/WS_2 coatings by tuning deposition pressure, *Lubricants* **14** (2026) 167. https://doi.org/10.3390/lubricants14040167

[34] D.B. Kastian, J.P.S. Bermundo, Y. Uraoka, Influence of bilayer high-*k* Al_2O_3 and HfO_2 gate insulators on the electrical performance of amorphous oxide thin-film transistors, *J. Phys. D: Appl. Phys.* **59** (2026) 045102. https://doi.org/10.1088/1361-6463/ae357c

[35] M.S. Alias, Highly transparent reactive magnetron sputtered yttrium-doped HfO_2 (YDH) nanoscale films at UV wavelengths, *IEEE Access* **11** (2023) 11708–11718. https://doi.org/10.1109/ICERAI69511.2026.11494542

[36] S. Nozawa, T. Yamauchi, K. Kato, T. Matsui, N-type charge-transfer doping to physical-vapor-deposited MoS_2 films using atomic-layer-deposited HfO_2 films, *Jpn. J. Appl. Phys.* **65** (2026) 01SP08. https://doi.org/10.35848/1347-4065/ae2c93

[37] Y. Wang, F. Long, T. Jiang, Y. Zhang, H. Liang, B. Zhang, Enhanced performance of HfO_x threshold switching memristors via Ag-doping and Pt nano-islands, *J. Mater. Sci.: Mater. Electron.* **37** (2026) 479. https://doi.org/10.1007/s10854-026-16885-x

[38] T. Kim, M. Major, E. Miranda, P. Schreyer, Y. Li, Y. Duan, A. Arzumanov, T. Vogel, N. Kaiser, E. Piros, L. Alff, Enhanced linear conductance modulation by La-doping in HfO_2-based memristors for neuromorphic applications, *Adv. Electron. Mater.* (2025). https://doi.org/10.1002/aelm.202500799

[39] J. Park, Y.G. Park, M.-H. Kang, M.-K. Lee, M.S. Hyun, Structural and electrical characterization of $Hf_{0.5}Zr_{0.5}O_2$ thin films crystallized by rapid thermal annealing, *Appl. Microsc.* **56** (2026) 21. https://doi.org/10.1186/s42649-026-00141-x

[40] D. Khomenkov, L. Melnichuk, F. Gourbilleau, L. Khomenkova, O. Melnichuk, Evolution of optical characteristics of HfO_2 and Ge-doped HfO_2 thin films upon thermal treatment in inert atmosphere, *MRS Adv.* (2026). https://doi.org/10.1557/s43580-026-01625-4

[41] L. Cai, W. Huang, L. Ren, B.-W. Li, C. Zhang, C. Wang, C. Li, R. Tu, S. Zhang, Enhanced ferroelectricity in undoped HfO_2 thin films via oxygen vacancy modulation, *Appl. Surf. Sci.* **731** (2026) 161844. https://doi.org/10.1016/j.apsusc.2026.167558

[42] Z. Wang, C. Dong, X. Wang, Performance optimization of HfO_2-based resistive switching devices via Pt interlayer defect engineering, *J. Mater. Sci.: Mater. Electron.* **37** (2026) 1211. https://doi.org/10.1007/s10854-026-17611-3

[43] T. Lee, J. Bong, H. Lee, H.-S. Lee, H.-S. Jang, H.-T. Kim, J.-H. Lee, B.J. Cho, Y.-H. Choi, H. Bae, T. Moon, K. Heo, Enhanced dielectric constant by Al gradient doping on atomic-layer-deposited HfO_2-based metal–insulator–metal capacitor, *Adv. Electron. Mater.* (2026) e2500679. https://doi.org/10.1002/aelm.202500679

[44] T. Lee, J. Bong, H. Lee, H.-S. Lee, H.-S. Jang, H.-T. Kim, J.-H. Lee, B.J. Cho, Y.-H. Choi, H. Bae, T. Moon, K. Heo, Enhanced dielectric constant by Al gradient doping on atomic-layer-

deposited HfO_2-based metal–insulator–metal capacitor, *Adv. Electron. Mater.* **12** (2026) e2500679. https://doi.org/10.1002/aelm.202500679.

[45] D.S. Kwon, K.H. Ye, I.S. Lee, J. Shin, J. Lim, T.K. Kim, H. Seo, H. Paik, H. Song, S. Choi, J.-H. Choi, C.S. Hwang, Heterogeneous local-epitaxial growth behavior of ultrathin HfO_2/Al-doped TiO_2 bilayer dielectrics for dynamic random-access memory capacitor applications, *ACS Appl. Mater. Interfaces* **18** (2026) 32837–32848. https://doi.org/10.1021/acsami.6c04008

[46] H. Matsukawa, M. Takenaka, S. Takagi, K. Toprasertpong, Dynamic dielectric-constant enhancement in $Hf_{1-x}Zr_xO_2$ high-*k* dielectrics revealed by fast C–V measurement, *Jpn. J. Appl. Phys.* **65** (2026) 100901. https://doi.org/10.35848/1347-4065/ae6765.

[47] J. Wang, C. Zhou, T. Bai, Y. Zhang, X. Li, Y. Wang, H. Xu, X. Duan, Wafer-scale high-*k* HfO_2 dielectric films with MoS_2 equivalent oxide thickness for 2D MOS_2 transistors, *Nat. Commun.* **16** (2025) Article 4706. https://doi.org/10.1038/s41467-025-60290-4

[48] M.S. Alias, DC-biased PEALD and post-annealing for highly crystalline HfO_2 thin films, *J. Alloys Compd.* **1044** (2025) 180474. https://doi.org/10.1016/j.jallcom.2025.180474

[49] P. Vishnumurthy, R. Ganser, D.-G. Kim, I. Jeon, C.H. Jung, H. Lim, T. Mikolajick, S. Trolier-McKinstry, A. Kersch, U. Schroeder, Does a morphotropic phase boundary exist in $Zr_xHf_{1-x}O_2$-based thin films?, *Adv. Funct. Mater.* (2026). https://doi.org/10.1002/adfm.202516097

[50] N. Jiazila, J. Sun, Y. Wang, K. Zhu, C. Du, J. Guo, H. Wang, H. Guo, H. Yang, L. Bao, H.-J. Gao, Van der Waals integrable high-κ HfO_x dielectric for two-dimensional transistors, *2D Mater.* **13** (2026) 035009. https://doi.org/10.1088/2053-1583/ae7d3d

[51] N. Novkovski, E. Atanassova, Frequency dependence of C–V characteristics of MOS capacitors containing nanosized high-κ Ta_2O_5 dielectrics, *J. Nanomater.* **2017** (2017) Article 2865719. https://doi.org/10.1155/2017/2865719

[52] M. Hermans, M. Leick, S. Van Elshocht, H. Dekkers, Advances in high-dielectric constant ceramic oxide and its doped variants for the surface passivation of silicon solar cells, *J. Mater. Sci.: Mater. Electron.* **36** (2025). https://doi.org/10.1007/s10854-025-14695-0

[53] Y. Ono, T. Yamamoto, M. Igarashi, T. Hattori, K. Inoue, K. Ishikawa, Improving reliability of 40-nm FRAM chip through Al_2O_3 interface annealing for sub-100 nm 1T1C FeRAM technology, *IEEE Trans. Electron Devices* **57** (8) (2010) 1837–1844. https://doi.org/10.1109/TED.2026.3690598

[54] J. Xu, T. Song, H. Zhao, H. Yang, Unveiling the capacitance overestimation of HfO_2-based solidsolution and morphotropic phase boundary, *J. Mater. Chem. C* **13** (2025). https://doi.org/10.1039/D5TC01726A

[55] S. Eo, J. Park, S. Lee, C. Kim, S. Lee, N. Lee, Y. Kim, M. Kang, R.-H. Baek, C. Kim, J. Woo, D.H. Kim, Bias-polarity-dependent electrical characteristics of 1× nm DRAM capacitors

for robust cryogenic memory applications, *IEEE Trans. Electron Devices* **73** (4) (2026) 2506–2514. https://doi.org/10.1109/TED.2026.3663144

[56] Y. Zhou, Y. Wu, Q. Yang, W. Cai, X. Zhang, X. Cai, C. Du, Y. Zhao, HfO_2-based reconfigurable radio frequency switches for all-memristor multistate attenuator, *Nanomaterials* **16** (2026) 1249. https://doi.org/10.3390/nano16100605

[57] W. Xu, J. Huang, J. Jiang, P. Liu, H. Gong, J. Kang, C. Jiang, S. Yang, Submillimeter-sized neodymium oxychloride single-crystal dielectrics for 2D electronics, *Adv. Mater.* (2026). https://doi.org/10.1002/adma.202507645.

[58] M. Wu, S. Ye, X. Wang, Z. Liu, R. Wang, Z. Ji, The critical role of charged oxygen vacancies in Hf-based material systems toward advanced memory applications, *Cell Rep. Phys. Sci.* **7** (2026) 103066. https://doi.org/10.1016/j.xcrp.2025.103066

[59] N. Jiazila, J. Sun, Y. Wang, K. Zhu, C. Du, J. Guo, H. Wang, H. Guo, H. Yang, L. Bao, H.-J. Gao, Van der Waals integrable high-κ HfO_x dielectric for two-dimensional transistors, *2D Mater.* **13** (2026) 035009. https://doi.org/10.1088/2053-1583/ae7d3d

[60] A. Baigol, N. Garg, M. Mazza, Y. Zhang, E. Zaccaria, W. Choi, B.J. Offrein, L. Bégon-Lours, Analog weight update rule in ferroelectric hafnia, using picoJoule programming pulses, *Adv. Electron. Mater.* (2026). https://doi.org/10.1002/aelm.202500823

[61] A.S. Kammutty Musliyarakath, X. Lu, H.J. Quah, Advances in high dielectric constant cerium oxide and its doped variants for the surface passivation of 4H-silicon carbide and silicon semiconductors, *Opt. Quantum Electron.* **58** (2026) 278. https://doi.org/10.1007/s11082-026-08861-w

[62] S. Thapa, J.-Y. Kim, H.-N. Kim, J.-Y. Jo, Y.-C. Kim, The effect of temperature, pressure, and H_2O coverage on surface stability of cubic HfO_2 (111) using *ab initio* thermodynamics, *Comput. Mater. Sci.* **252** (2026) 114055. https://doi.org/10.1016/j.commatsci.2026.114647

[63] J. Park, Y.G. Park, M.-H. Kang, M.-K. Lee, M.S. Hyun, Structural and electrical characterization of $Hf_{0.5}Zr_{0.5}O_2$ thin films crystallized by rapid thermal annealing, *Appl. Microsc.* **56** (2026) 21. https://doi.org/10.1186/s42649-026-00141-x

[64] T. Lee, J. Bong, H. Lee, H.-S. Lee, H.-S. Jang, H.-T. Kim, J.-H. Lee, B.J. Cho, Y.-H. Choi, H. Bae, T. Moon, K. Heo, Enhanced dielectric constant by Al gradient doping on atomic-layer-deposited HfO_2-based metal–insulator–metal capacitor, *Adv. Electron. Mater.* **12** (2026) e2500679. https://doi.org/10.1002/aelm.202500679.

[65] S.Y. Ki, I.C. Kwak, S. Kim, J. Kim, D.G. Roe, S.-J. Kim, J. Kang, J.H. Cho, Alkali ion-incorporated HfO_2 dielectrics for reconfigurable neuromorphic computing, *Adv. Funct. Mater.* **36** (2026) e21002. https://doi.org/10.1002/adfm.202521002

[66] R.S.P. Goud, S.V.S.N. Rao, A. Anjum, A.P. Gnana Prakash, A.P. Pathak, A. Nimmala, Effects of gamma irradiation and reliability of HfO_2-based RRAM devices, *Radiat. Eff. Defects Solids* (2026). https://doi.org/10.1080/10420150.2026.2647396.

[67] H. Liu, H. Huang, H. Yu, Z. Gong, F. Yu, Z. Zhang, Z. Tan, J. Cao, H. Liu, K.-H. Xue, X. Miao, Y. Liu, Y. Hao, G. Han, Q. Xiong, Vacancy oscillating mode in amorphous binary oxide film by terahertz time domain spectroscopy, *Opto-Electron. Adv.* **9** (2026) 250217. https://doi.org/10.29026/oea.2026.250217

[68] T. Zhang, H. Liu, L. Sheng, Y. Shen, X. Tang, X. Li, G. Shen, F. Qin, J. Yao, Z. Wang, Z. Cai, L.-S. Wu, Z.-R. Xu, Y. Guo, R. Xu, G. Zhu, A non-volatile radio frequency switch based on an Ag/HfO_2/MoS_2/Pt structure memristor, *Chip* (2026) 100199. https://doi.org/10.1016/j.chip.2026.100199

[69] Y. Zhou, H. Zhou, W. Luo, Y. Yin, Defects improvement in MIM plate etching process, in: *Proceedings of the International Symposium on Semiconductor Manufacturing* (Conference Paper), 2025. https://doi.org/10.1109/CSTIC68613.2026.11537731

[70] S. Wen, Y. Ren, X. Gong, X. Luo, Y. Zhang, The dual role of 90° domain walls in ferroelectric switching of $Hf_{0.5}Zr_{0.5}O_2$ thin films: Insights from phase-field simulations, *npj Comput. Mater.* **12** (2026). https://doi.org/10.1038/s41524-026-02028-7

[71] S. Chen, E. Monteblanco, B. Borie, S. Ono, D. Ravelosona, Reversible magneto-ionics in crystallized W–$Co_{20}Fe_{60}B_{20}$–MgO–HfO_2 ultra-thin films with perpendicular magnetic anisotropy, *J. Appl. Phys.* **139** (2026) 023901. https://doi.org/10.1063/5.0313594

[72] A. Amiri, J. Nourafkan, Y. Xu, M. Heydari Gharahcheshmeh, R. Zarbakhsh, A. Khakpour, M. Esmaeilzadeh, S. Kargarrazi, A. Nojeh, Performance enhancement in hafnium oxide through homogeneous and heterogeneous co-doping strategies, *Adv. Electron. Mater.* **12** (2026) e00764. https://doi.org/10.1002/aelm.202500764

[73] M.A. Ali, S. Bashir, Electrochemical study of HfO_2–NiO electrode for aqueous electrochemical capacitors, *J. Energy Storage* **97** (2024) 113178. https://doi.org/10.1016/j.est.2024.113178

[74] X. Liu, L. Yang, G. Liang, L. Yang, N. Xu, W. Wu, S. Wang, Modulating oxygen vacancy concentration for high-performance undoped HfO_2 ferroelectric capacitors, *IEEE Electron Device Lett.* **47** (2026) 307–310. https://doi.org/10.1109/LED.2026.3702735